Rimonabant, a potent CB1 cannabinoid receptor antagonist, is a $G\alpha_{i/o}$ protein inhibitor.

Alessandra Porcu[a,b], Miriam Melis[a], Rostislav Turecek[b], Celine Ullrich[b], Ignazia Mocci[c], Bernhard Bettler[b], Gian Luigi Gessa[a,d,e,f*] and M. Paola Castelli[a,f*]

[a]Department of Biomedical Sciences, University of Cagliari, 09042-Monserrato, Italy

[b]Department of Biomedicine, University of Basel, Klingelbergstrasse 50-70, CH-4056 Basel, Switzerland

[c]Institute of Translational Pharmacology, National Research Council of Italy (CNR) U.O.S. of Cagliari, 09010-Pula, Italy.

[d]Guy Everett Laboratory, University of Cagliari, 09042-Monserrato, Italy

[e]Neuroscience Institute, National Research Council of Italy (CNR), Cagliari, Italy

[f]Center of Excellence "Neurobiology of Addiction", University of Cagliari, 09042-Monserrato, Italy

Corresponding author:

M. Paola Castelli, MD, PhD,
Department of Biomedical Sciences
Division of Neuroscience and Clinical Pharmacology,
Cittadella Universitaria, SS 554, km. 4,500,
I-09042 Monserrato (CA), ITALY.
Telephone: +39-070-6754065;
FAX: +39-070-6754320,
e-mail:castelli@unica.it

[*]These authors contributed equally to the study

Abbreviations

BRET, Bioluminescence resonance energy transfer

CAMYEL, cAMP sensor using YFP-EPAC-Rluc

CB1, Cannabinoid receptor type 1

CB1-KO, CB1-knock out

CNS, Central nervous system

CHO, Chinese Hamster Ovary, CHO

GDP, Guanosine 5′-diphosphate

GIRK, G-protein-coupled inwardly rectifying K^+ channels

GPCR, G-protein coupled receptor

GTPγS, guanosine 5'-O-(3-thiotriphospate)

HEK-293, Human Embryonic Kidney 293

ABSTRACT

Rimonabant is a potent and selective cannabinoid CB1 receptor antagonist widely used in animal and clinical studies. Besides its antagonistic properties, numerous studies have shown that, at micromolar concentrations rimonabant behaves as an inverse agonist at CB1 receptors. The mechanism underpinning this activity is unclear. Here we show that micromolar concentrations of rimonabant inhibited $G\alpha_{i/o}$-type G proteins, resulting in a receptor-independent block of G protein signaling. Accordingly, rimonabant decreased basal and agonist stimulated [^{35}S]GTPγS binding to cortical membranes of CB1- and $GABA_B$-receptor KO mice and Chinese Hamster Ovary (CHO) cell membranes stably transfected with $GABA_B$ or D2 dopamine receptors. The structural analog of rimonabant, AM251, decreased basal and baclofen-stimulated GTPγS binding to rat cortical and CHO cell membranes expressing $GABA_B$ receptors. Rimonabant prevented G protein-mediated $GABA_B$ and D2 dopamine receptor signaling to adenylyl cyclase in Human Embryonic Kidney 293 cells and to G protein-coupled inwardly rectifying K^+ channels (GIRK) in midbrain dopamine neurons of CB1 KO mice. Rimonabant suppressed GIRK gating induced by GTPγS in CHO cells transfected with GIRK, consistent with a receptor-independent action. Bioluminescent resonance energy transfer (BRET) measurements in living CHO cells showed that, in presence or absence of co-expressed $GABA_B$ receptors, rimonabant stabilized the heterotrimeric Gαi/o-protein complex and prevented conformational rearrangements induced by $GABA_B$ receptor activation. Rimonabant failed to inhibit Gαs-mediated signaling, supporting its specificity for $G\alpha_{i/o}$-type G proteins. The inhibition of $G\alpha_{i/o}$ protein provides a new site of rimonabant action that may help to understand its pharmacological and toxicological effects occurring at high concentrations

Key words: Bioluminescence resonance energy transfer (BRET), cannabinoid receptor type 1 (CB1), CB1-receptor antagonist, inverse agonist, G protein, G protein-coupled receptor (GPCR)

1. Introduction

Heterotrimeric guanine nucleotide binding proteins (G proteins) are primarily activated by G protein coupled receptors (GPCRs) that transduce extracellular stimuli from the cell surface to intracellular signaling cascades (Milligan and Kostenis, 2006; Denis et al., 2012; Syrovatkina et al., 2016). G protein signaling is regulated by "the regulator of G-protein-signaling" (RGS) proteins that activate the GTPase activity of the Gα subunits (Sato et al., 2006; Roman 2009; Sjögren et al., 2010, 2011). RGS proteins are, therefore, potential targets for therapeutic agents intended to prolong and enhance receptor-induced G protein signaling. There is also evidence that Gα or Gβγ subunits of the heterotrimeric G protein can be directly targeted by small molecules with potential therapeutic action (see Smrcka 2013 for a review). For example, the anti-helminthic drug suramin and some of its analogues were found to inhibit the exchange of GDP for GTP at Gα subunit (Smrcka 2013). Likewise, the cyclic depsipeptide YM-254890 stabilizing the GDP bound form of $G\alpha_q$ subunit (Freissmuth et al., 1996; Takasaki et al., 2004). This compound delineates a target site for the development of inhibitors of G protein signaling, which would be of therapeutic benefit in ovarian cancer treatment (Nishimura et al., 2010, Kan et al. 2010). Moreover, fluorescein analogues that bind with micromolar affinity to Gβγ subunit have been identified; one of these potentiated morphine analgesia in rats (Bonacci et al., 2006). Recently, Ayoub et al. (2009) have identified two imidazopyrazine derivatives (BIM-46174 and BIM-46187) that prevented the GPCR-induced activation of all the G protein families tested. The compound BIM-46174 displayed anti-proliferative activity while the compound BIM-46187, which binds to the $G\alpha_{i2}$ subunit, induced pain relief (Prévost et al. 2006; Favre-Guilmard et al. 2008).

Rimonabant, (SR, 141716A (*N*-(Piperidin-1-yl)-5-(4-chlorophenyl)-1-(2,4-dichlorophenyl)-4-methyl-1*H*-pyrazole-3-carboxamide hydrochloride) is a highly potent and selective cannabinoid receptor (CB1) antagonist (Ki= 1.98 nM) (Rinaldi-Carmona et al., 1994) that displays a plethora of pharmacological effects under several pathophysiological conditions, including obesity-related disorders (Van Gaal et al., 2005; Scheen et al., 2006; Pi-Sunyer et al. 2006; Padwal and Majuumdar 2007; Xie et al., 2007), drug addiction (i.e., alcohol, nicotine) (Le Foll et al., 2008; Soyka et al., 2008; Beardsley et al., 2009; Cahill and Ussher 2011) and anticancer effects *in vitro* (Flygare et al., 2005; Bifulco et al., 2007; Malfitano et al., 2007; Ciaglia et al., 2015). Rimonabant was approved as an anti-obesity treatment (Acomplia, European Public Assessment Report 2007) in more than 50 countries worldwide. Rimonabant counteracts an increased tone of endogenous cannabinoids responsible for excessive appetite and metabolic alterations associated with obesity. While the efficacy of rimonabant in weight reduction was demonstrated in a series of major reports, the meta-analysis of clinical studies has revealed that its beneficial effect on obesity was associated with adverse psychiatric events, including anxiety and depression, increased risk of suicidal ideation and suicide attempts (Christensen et al., 2007; Rucker et al.,

2007; Moreira et al., 2009). Due to these adverse effects rimonabant was withdrawn from the market in 2009.

Besides being a potent and selective CB1 receptor antagonist, rimonabant at nanomolar concentrations exhibits CB1-dependent inverse agonistic effects, including the inhibition of basal GTPγS binding (Lansdsman et al., 1997; MacLennan et al., 1998; Pertwee 2005; Howlett et al., 2011). In addition, numerous studies indicated that rimonabant at micromolar concentrations reliably inhibits GTPγS binding also in the presence or absence of CB1 receptors, both, in rodent and human brain tissues as well as in heterologous system (Sim-Selley et al., 2001; Breivogel et al., 2001; Savinainem et al., 2003; Cinar and Szücs 2009; Erdozain et al., 2012, Pertwee 2005). Several explanations have been proposed for the CB1-independent inverse agonist activity of rimonabant, but the mechanism is still highly debated (Pertwee 2005; Howlett et al., 2011; Raffa and Ward 2012).

Here we demonstrate that at micromolar concentrations, higher than those commonly used to block the CB1 receptor, rimonabant inhibited activation of heterotrimeric G protein by acting at the $G\alpha_{i/o}$ subunit. Accordingly, rimonabant produced a receptor-independent reduction of basal activity of $G\alpha_{i/o}$, prevented GPCR-mediated activation of $G\alpha_{i/o}$ proteins and signaling to their effectors. BRET experiments support that rimonabant induced conformational changes in heterotrimeric G protein. Our study identifies a new site of action of rimonabant thereby indicating that micromolar concentrations inhibit $G_{\alpha i/o}$-type G proteins.

2. Matherial and Methods

2.1 Animals—All procedures and experiments were carried out according to Italian (D.L. 26/2014) and European Council directives (63/2010) and in compliance with the approved animal policies by the Ethical Committee for Animal Experiments (CESA, University of Cagliari) and the Italian Department of Health. All possible efforts were made to minimize animal pain and discomfort and to reduce the number of experimental subjects. Male Sprague Dawley rats and DBA mice (Harlan Nossan, San Pietro al Natisone, Italy), weighing 200 to 250 and 17 to 20 g, respectively, were used. $GABA_{B1}$ knockout ($GABA_{B1}$-KO) and CB1-KO mice were obtained and genotyped as previously described (Schuler et al., 2001; Marsicano et al., 2002). Rats and mice were housed 4 and 6 per cage, respectively, in a temperature- and light-controlled room. Light was on a 12-h cycle, and food and water were available ad libitum.

2.2 Drugs and plasmid constructs—Guanosine 5′-diphosphate (GDP) and guanosine 5′-O-(3-thiotriphosphate) (GTPγS) were purchased from Sigma/RBI (St.Louis, MO, USA). [^{35}S]GTPγS (125 Ci/mM) and [^{3}H]CGP54626 (85 Ci/mM) were obtained from PerkinElmer and American Radiolabeled Chemicals Inc. (St. Louis, MO, USA), respectively. Luciferase substrate, Coelenterazine, was purchased

from NanoLight Technologies (US), Lipofectamine 2000 transfection reagents were obtained from Thermo Fisher Scientific (Waltham, MA). CGP54626, (*R*)-baclofen, quinpirole and A68293 were purchased from Tocris Bioscience (Ellisville, MO, USA). Rimonabant was a generous gift from G. Le Fur (Sanofi-Aventis Recherche, France), while the structural analog AM251 *N*-(Piperidin-1-yl)-5-(4-iodophenyl)-1-(2,4-dichlorophenyl)-4-methyl-1*H*-pyrazole-3-carboxamide was purchased from Tocris Bioscience (Ellisville, MO, USA). Drugs were dissolved in 100 % DMSO and then diluted in an assay buffer. The concentration of DMSO used in the different assays never exceeded 0.1% (v/v) and had no effects on [^{3}H]CGP54626 and [^{35}S]GTPγS binding assay, electrophysiological recordings and BRET measurements. Specifically, rimonabant or other drugs were dissolved at a concentration of 0.1 M in 100% DMSO (stock solution) and diluted in buffer to obtain the working solution, i.e. dilution 1/1000 to obtain the final concentration of 0.0001 M of drug in buffer containing 0.1 % of DMSO.
The plasmid pcDNA3L-His-(cAMP sensor using YFP-Epac-RLuc) (CAMYEL, MBA-277) (Jiang et al., 2007) was purchased from ATCC.

$G\alpha_o$-Rluc, $G\gamma_2$-Venus, $G\beta_1$-Flag, Gγ2-HAwere a kind gift from Jean Philippe Pin (Institute of Functional Genomics, Montpellier, France), myc-$GABA_{B1a}$ and myc-$GABA_{B2}$ were obtained as previously described (Pagano et al., 2001). The $G\beta_1$-Rluc and $G\gamma_2$-Rluc constructs were produced by inserting the coding sequence of humanized Rluc into $G\beta_1$ and $G\gamma_2$ (Fritzius et al., 2016). HA-D1 and HA-D2 encoding for the human D1dopamine receptor and for the mouse D2 dopamine long receptor, respectively, were a kind gift from Bernd Fakler (University of Freiburg, Freiburg, Germany). $G\alpha_{i1}$ 91-Venus, $G\alpha_{i1}$ 121-Venus and $G\alpha_{i1}$ 60-Venus constructs, which consisted in Venus A206K inserted between residues 60 and 61, 91 and 92 or 121 and 122 of human $G\alpha_{i1}$ C351G were a kind gift from Nevin Lambert (Medical College of Georgia, Augusta, USA).

2.3 Cell culture and transfection of CHO-K1 and HEK-293 cells—For the [^{35}S]GTPγS binding assay, CHO-K1 cells were cultured to 80% confluency ($3x10^6$ cells in 100-mm dishes) in DMEM supplemented with 500 µM L-glutamine (Sigma-Aldrich, Milan, Italy) and 10% FBS in a humidified atmosphere of 5% CO_2 at 37°C. Then cells were incubated for 6 h with 30 µg of pcDNA3.1 (Zeo) plasmid containing the cDNA encoding for the human D2 dopamine long receptor (a kind gift from Olivier Civelli, Dept. of Pharmacology, University of California, USA) and 60 µl of Lipofectamine reagent in serum-free Opti-MEM. Selection antibiotic (300 µg/ml zeocin) was added to the cell culture medium 48 h after transfection, and surviving colonies were harvested 14 days later. To confirm D2 long expression, competition and saturation binding experiments using [^{3}H]YM09151-2, aspecific D2 receptor antagonist, were performed as previously described (Vanhauwe et al., 1999). The clone expressing the highest level of D2 receptors was selected and designated CHO-D2, maintained in DMEM containing 300µg/ml zeocin

and used throughout the study. For BRET measurements, culture and maintenance of CHO-K1 cells stably expressing $GABA_{B1b}$ and $GABA_{B2}$ (CHO-$GABA_B$) were performed and maintained as described (Urwyler et al., 2001). HEK-293 cells were cultured in DMEM supplemented with 10% FBS in a humidified atmosphere of 5% CO_2 at 37°C. Transient transfections in CHO-$GABA_B$ and HEK-293 were performed with different plasmids encoding RLuc and YFP fusion proteins (see figure legends) and were carried out using Lipofectamine 2000 according to the manufacturer's protocol.

2.4 Binding studies

2.4.1 [^{35}S]GTPγS binding assay in rat/mice membranes and in CHO, CHO-$GABA_B$ and CHO-D2 cell membranes—$GABA_B$-stimulated [^{35}S]GTPγS binding in rat/mice membranes was carried out as previously described (Castelli et al., 2012). For CB1-stimulated [^{35}S]GTPγS binding, cortical membranes (10-15 µg of proteins) were incubated in an assay buffer (50 mM Tris-HCl, 3 mM $MgCl_2$, 0.2 mM EGTA and 100 mM NaCl, BSA 0.1%, pH 7.4) at 30°C for 1 h with 30 µM GDP and 0.05 nM [^{35}S]GTPγS in a final volume of 1 ml. After incubation, the samples were filtered using a PerkinElmer UniFilter-GF/B, washed twice with 1 ml of buffer and dried for 1 h at 30°C. For D2-stimulated [^{35}S]GTPγS binding, striatal membranes (20 µg of proteins) were pre-incubated in an assay buffer (20 mM K-HEPES, 7 mM $MgCl_2$, 1 mM EDTA, 1mM DTT and 100 mM NaCl, pH 7.6) at RT for 30 min with 300 µM GDP. The main incubation was subsequently started by the addition of [^{35}S]GTPγS to a final concentration of 0.1 nM in a volume of 300 µl. After 60 min of incubation at 35 °C, the samples were filtered using a PerkinElmer UniFilter-GF/B, washed twice with 1 ml of buffer (20 mM K-HEPES and 100 mM NaCl, pH 7.6), and dried for 1 h at 30°C. For CHO-$GABA_B$ stimulated [^{35}S]GTPγS binding, membranes (20 µg of proteins) were incubated in an assay buffer (50 mM Tris-HCl, 10 mM $MgCl_2$, 0.2 mM EGTA and 100 mM NaCl, 2 mM $CaCl_2$, pH 7.7) at 22-24°C for 1 h with 30 µM GDP and 0.2 nM [^{35}S]GTPγS in a volume of 0.3 ml. After incubation, the samples were filtered using a PerkinElmer UniFilter-GF/C, washed twice with 1 ml of buffer and dried for 1 h at 50°C (Urwyler et al. 2001). For CHO-D2 and CHO non-transfected cells stimulated [^{35}S]GTPγS binding, membranes (10 µg of proteins) were pre-incubated in an assay buffer (50 mM K-HEPES, 10 mM $MgCl_2$,100 mM NaCl, 0.1% BSA, pH 7.4) for 30 min at 30°C with 10 µM of GDP. The main incubation was subsequently started with the addition of [^{35}S]GTPγS to a final concentration of 0.1 nM. After 90 min incubation at 30°C, the samples were filtered using a PerkinElmer UniFilter-GF/B, washed twice with 300 µl of buffer 50 mM HEPES, pH 7.4, and dried for 1 h at 30°C. The radioactivity on the filters was counted in a liquid microplate scintillation counter (TopCount NXT; PerkinElmer Life and Analytical Sciences) using 50 µl of scintillation fluid (Microscint 20; PerkinElmer Life and Analytical Sciences). The stimulation by the agonist was defined as the percentage increase above basal levels (i.e. [disintegrations per minute (agonist) - disintegrations per minute (no

agonist)/(disintegrations per minute (no agonist)] × 100). Data are reported as the mean SEM of three to six experiments, performed in triplicate. Nonlinear regression analysis of concentration-response data was performed using Prism 2.0 software (Graph Pad Prism) to calculate Emax and EC_{50} values.

2.5 BRET Measurements

2.5.1 BRET measurements of G-protein activity in CHO-GABA$_B$ and in HEK-293 cells—CHO-$GABA_B$ cells were transfected with plasmids encoding $G\alpha_o$-Rluc, $G\gamma_2$-Venus, $G\beta_1$-Flag and after 6 h were seeded into 96-well microplates (Costar Corning Incorporated; coated with poly-L-ornithine hydrobromide; P3655, Sigma-Aldrich). HEK-293 cells were transiently transfected with plasmids encoding Rluc and YFP fusion proteins (see figure legends) and after 6 h were plated into 96-well microplates. 24 h after transfection, both the transfected CHO-$GABA_B$ and the HEK-293 cells were washed twice with PBS, and incubated at 37°C for 1 h with PBS containing rimonabant or the vehicle. Measurement was initiated using an Infinite® F500 microplate reader (Tecan, Switzerland) after 10 minutes of incubating the luciferase substrate (5 µM, Coelenterazine h, NanoLight Technologies). Baclofen (10 µM) was applied after 29 cycles of reading (≈25 sec) to CHO-$GABA_B$ cells. Luminescence and fluorescence signals were detected sequentially with an integration time of 200 ms. The BRET ratio was calculated as the ratio of light emitted by Venus (530–570 nm) over the light emitted by RLuc (370–470 nm) and corrected by subtracting ratios obtained with the Rluc fusion protein alone. The results were expressed in mBRET units (BRET x 1000). The curves were fitted using GraphPad Prism 5.0 ("plateau followed by one-phase decay"). ΔBRET was calculated as the difference between the basal and the plateau of the BRET signal.

2.5.2 BRET measurements of cAMP responses using the YFP-Epac-RLuc (CAMYEL) sensor—HEK-293 cells were transiently co-transfected with pcDNA3L-His-CAMYEL and with myc-$GABA_{B1a}$ and myc-$GABA_{B2}$, or with HA-D2, or HA-D1 plasmids. 6 h later, cells were distributed into 96-well microplates, and 24 h after transfection, were washed twice with PBS and pre-incubated at 37°C for 1 h with PBS containing rimonabant or the vehicle. The measurement was initiated using the Infinite® F500 microplate reader (Tecan, Switzerland) after 10 minutes of incubation with the luciferase substrate (5 µM, Coelenterazine). On HEK-293 transfected with $GABA_B$ or D2 receptor, forskolin (0.5 µM) was applied after 150 seconds of reading to stimulate cAMP production. Then, either baclofen (10 µM) or quinpirole (10 µM) was applied after 500 seconds of reading. On HEK-293 transfected with D1 receptor A68293 was applied after 150 seconds of reading. Luminescence and fluorescence signals were detected sequentially with an integration time of 200 ms. The BRET ratio was calculated as the ratio of light emitted by YFP (530–570 nm) over the light emitted by RLuc (370–470 nm). The curves were fitted using GraphPad

Prism 5.0 (“plateau followed by one-phase decay or by one-phase association”). ΔBRET was calculated as the difference between the basal and the plateau of the BRET signal.

2.6 Electrophysiology

2.6.1 Whole-cell voltage clamp recordings from dopamine neurons— Whole-cell patch-clamp recordings from midbrain dopamine cells were as previously described (Melis et al. 2010). Briefly, male Sprague Dawley rats or CB1-KO out mice were anesthetized with halothane and killed. Recordings were made from horizontal slices superfused with artificial cerebrospinal fluid (ACSF, 37° C), saturated with 95% O_2 and 5% CO_2 containing (in mM): 126 NaCl, 1.6 KCl, 1.2 NaH_2PO_4, 1.2 $MgCl_2$, 2.4 $CaCl_2$, 18 $NaHCO_3$ and 11 glucose. Voltage-clamp experiments were performed with electrodes filled with a solution containing the following (in mM): 144 KCl, 10 HEPES, 3.45 BAPTA, 1 CaCl, 2.5 Mg_2ATP, and 0.25 Mg_2GTP (pH 7.2–7.4, 275–285 mOsm). Experiments began after series resistance had stabilized (typically 15–40 MΩ). Series and input resistance were continuously monitored on-line with a 5 mV depolarizing step (25 ms). Data were filtered at 2 kHz, digitized at 10 kHz, and collected on-line with acquisition software (pClamp10.6, Molecular Devices). Dopamine neurons from lateral portion of posterior VTA were identified by the presence of a large I_h current (Johnson et al., 1992) that was assayed immediately after break-in using a series of incremental 10 mV hyperpolarizing steps from a holding potential of -70 mV. Each slice received one single drug exposure. All the drugs were dissolved in DMSO. The final concentration of DMSO was < 0.01 %. Statistical significance was assessed using a paired *t* test (with Welch’s correction).

2.6.2 Whole-cell patch-clamp recordings from CHO cells—CHO cells were transfected with cDNAs encoding the GIRK 1/2 concatemer (Kaupmann et al., 1998) using Lipofectamine 2000 (Invitrogen) according to the manufacturer’s instructions. 48 h after transfection experiments on CHO cells were performed at room temperature as previously described (Turecek et al., 2014). During recording, CHO cells were continuously superfused with an extracellular solution composed of (in mM): 145 NaCl, 2.5 KCl, 1 $MgCl_2$, 2 $CaCl_2$, 10 HEPES, 25 Glucose; pH 7.3, 323 mOsm. Patch pipettes had resistances between 3-4 MΩ when filled with intracellular solution composed of (in mM) 107.5 potassium gluconate, 32.5 KCl, 10 HEPES, 5 EGTA, 4 Mg ATP, 0.6 $Li_4GTP\gamma S$, 10 Tris phosphocreatine; pH 7.2, 297 mOsm. Series resistance (< 5 MΩ) was compensated by 80%. Kir3 responses induced by GTPγS were recorded with an Axopatch 200B patch-clamp amplifier (Molecular Devices, USA); filtering and sampling frequencies were set to 1 kHz and 5 kHz, respectively. Data analyses were done with pClamp 10 (Molecular Devices, USA). Data are given as mean ± SD. Statistical significance was assessed using a t-test. Rimonabant was dissolved in 100% DMSO and then diluted in an extracellular solution at a final

concentration of 10 μM. The final concentration of DMSO was 0.1 %, which was the same in the vehicle. Before the recording, CHO cells were pre-incubated in the extracellular solution either in the presence of the drug or the vehicle for 45 minutes at room temperature (22 - 24°C).

2.7 Statistical Analysis—Data were expressed as the mean ± SEM and statistically evaluated by an unpaired *t*-test or by one-way ANOVA followed by the Bonferroni or Tukey test for multiple comparisons with significance for $p < 0.05$.

3 RESULTS

3.1 Rimonabant inhibits constitutive and agonist stimulated G protein activity—The effects of rimonabant on G protein basal activity was evaluated using [^{35}S]GTPγS binding assays in striatal or cortical membranes of rodents and membranes of CHO cells stably transfected with $GABA_B$ or D2 receptor as well as untransfected CHO cells. As shown in Table 1, rimonabant dose dependently reduced basal [^{35}S]GTPγS binding with a similar potency to cortical and striatal membranes of rats, as to cortical membranes of both CB1-KO and $GABA_B$-KO mice and their wild-type littermates. Rimonabant also decreased, in a concentration-dependent manner, G protein basal activity in CHO cells expressing the $GABA_B$ or D2 receptor and in untransfected CHO cells (Table 1). Neither the $GABA_B$ receptor agonist baclofen (100 μM) nor the CB1 receptor agonist CP55,940 (100 μM) had any effect on [^{35}S]GTPγS binding in untransfected CHO cell membranes, indicating that CHO cells do not express endogenous $GABA_B$ or CB1 receptors (data not shown). The inhibitory effect of rimonabant was observed at concentrations of GDP and NaCl that allow a constant and significant reduction in basal [^{35}S]GTPγS, as previously reported (Sim-Selley et al., 2001). However, in contrast to previous studies (Lansdsman et al., 1997; MacLennan et al., 1998; Howelett et al., 2011), rimonabant at 10 and 100 nanomolar concentrations failed to inhibit basal [^{35}S]GTPγS binding (100.3 % ± 2 and 93 % ± 5 over basal activity, respectively). The effect of rimonabant on the stimulation of [^{35}S]GTPγS binding by baclofen and the D2 receptor agonist quinpirole was measured in rat and mouse cortical membranes. As shown in Fig. 1A at 5 μM concentration rimonabant induced a rightward shift in the concentration-response curve of baclofen-induced stimulation of [^{35}S]GTPγS binding, resulting in a significant increase in EC_{50} (Table 2). However, while this concentration had no effect on the maximal efficacy (Emax) of baclofen (Table 2), both the potency and the Emax were reduced by a concentration of 25 μM (Suppl. Fig. 1). The pEC50 moved from 5.15 ± 0.06 (EC_{50} = 7.30 ± 1.10 μM) to 3.95 ± 0.10 (EC_{50} = 119 ± 24.85 μM) ($p < 0.05$ and $p < 0.001$, respectively) and the Emax was reduced from 201 ± 10 % to 132 ± 7 % ($p < 0.05$).

An increase in the EC_{50} of baclofen was also observed with 5 μM of rimonabant in cortical membranes of CB1-KO mice (Fig. 1B, Table 2) and of its wild-type littermates (data not shown). These results indicate that the inhibitory effect of rimonabant on baclofen-induced G protein activation is CB1 receptor-independent. Moreover, similarly to what observed with baclofen, 5 μM rimonabant reduced the potency of quinpirole in inducing [^{35}S]GTPγS binding (Fig. 1C, Table 2), but failed to modify quinpirole efficacy. Altogether, these data confirmed that the inhibitory effect of rimonabant on $G_{i/o}$ protein activity is not selective for a particular GPCR. Moreover, up to a concentration of 1 mM, rimonabant failed to inhibit the binding of the specific $GABA_B$ receptor antagonist [^{3}H]CGP54626 to rat cortical membranes (data not shown), ruling out the action of rimonabant at the $GABA_B$ receptor itself.

As fig. 2 shows, the structural analog of rimonabant AM251 at 10 μM significantly decreases basal GTPγS binding both in rat cortical (Fig 2A) and in CHO cell membranes stably expressing $GABA_B$ receptors (Fig 2B). Moreover, as shown in Fig. 2C, in rat cortical membranes AM251 also inhibited the [^{35}S]GTPγS stimulation induced by a submaximal concentration (10 μM) of the $GABA_B$ receptor agonist baclofen. No significant difference in the ability to decrease basal and $GABA_B$-stimulated G protein activity was observed between AM251 and rimonabant.

Next, we used a BRET approach in CHO-$GABA_B$ cells to evaluate the influence of rimonabant on the conformational changes between $G\alpha_o$-RLuc and $G\gamma_2$-Venus before and after $GABA_B$ receptor activation (Fig. 3A). As shown in Fig. 3B and C, rimonabant increased the basal BRET signal measured between $G\alpha_o$-RLuc and $G\gamma_2$-Venus subunits in a concentration-dependent manner. Additionally, rimonabant reduced the magnitude of BRET changes during baclofen-induced G protein dissociation (Suppl. Fig. 2A) in a concentration-dependent manner, thus leading to a significant decrease in ΔBRET (Fig. 3D). These data suggest that rimonabant, independently of $GABA_B$ receptor activation, stabilizes the heterotrimeric state of the G protein and inhibits G protein activation. These effects of rimonabant were specific, since it did not directly alter Rluc activity for the duration of the experiments, even at a concentration of 50 μM (Suppl. Fig 2B).

3.2 Rimonabant inhibits GPCR signaling pathways—The effect of rimonabant on the signaling of $GABA_B$ and D2 receptors, which share a pool of $G_{i/o}$ proteins, was evaluated by monitoring in real time intracellular cAMP production in living cells using the CAMYEL sensor (Jiang et al. 2007; Porcu et al., 2016). BRET signal was recorded for 150 seconds to monitor basal cAMP production in HEK-293 cells co-transfected with CAMYEL and $GABA_B$ receptor (Fig 4A). Forskolin (0.5 μM) was added to stimulate cAMP production, resulting in a conformational change in the CAMYEL recorded as a decrease in BRET. The addition of baclofen reduced forskolin-stimulated cAMP production, as indicated by the increase in BRET. Rimonabant reduced baclofen-mediated inhibition of cAMP production, corresponding to a faster

and enhanced CAMYEL activation compared to the control (vehicle-pretreated), as indicated by the decrease in the time constant (*t*) of CAMYEL activation (Fig. 4B) and ΔBRET (Fig. 4C).

As observed for the $GABA_B$ receptor, rimonabant also reduced the quinpirole-induced *t* of CAMYEL activation and ΔBRET, indicating that it decreased the quinpirole-induced inhibition of cAMP formation in HEK-293 cells expressing the D2 receptor (Fig. 4D-F). These results indicate that rimonabant reduces $G_{i/o}$ mediated inhibition of cAMP production induced by $GABA_B$ and D2 receptor agonists. Moreover, rimonabant did not significantly alter ($p>0.05$ vs vehicle-pretreated) the forskolin-induced BRET signal before baclofen or quinpirole stimulation, indicating that it does not directly inhibit adenylyl cyclase but instead inhibits $G_{i/o}$-protein signaling. To address whether rimonabant specifically inhibits $G_{i/o}$-proteins, its effect on Gs-mediated cAMP activation by the D1 selective receptor agonist A68293 was evaluated. In HEK-293 cells co-expressing the CAMYEL and the D1 receptor, rimonabant failed to modify A68293-induced activation of cAMP as measured by a decrease in BRET (Fig. 5) indicating that rimonabant does not inhibit $G\alpha_s$-dependent cAMP formation.

Whole-cell voltage-clamp ($V_{holding}$= -70 mV) recordings from midbrain dopamine neurons in acute rat brain slices *ex vivo* were performed to evaluate the effects of rimonabant on baclofen- and quinpirole-induced outward K^+ currents (Lacey et al., 1988; Jiang et al., 1993). As shown in Fig. 6A, baclofen application (10 μM) induced an outward K^+ current activated by the $GABA_B$ receptor (160.5± 29 pA, n=6) that is reproducible upon repeated applications over time (Lacey et al., 1988; Jiang et al., 1993). However, when the slice was pretreated with rimonabant (10 μM), baclofen- induced outward current was abolished (31.7± 26.9 pA, n=6; p= 0.004; Fig. 6B). The CB1 receptor was not required for the rimonabant-induced blockade of $GABA_B$-induced current, since rimonabant also prevented the baclofen-induced current in CB1-KO mice (14.7± 8.6 vs. 134.9± 6.6 pA in the presence and absence of rimonabant, respectively; n=3, p=0.0002; Fig. 6C). Moreover, rimonabant pretreatment abolished the D2 receptor-mediated outward current induced by quinpirole (1 μM) bath application (143.0± 41.4 vs. 13.9± 8.0 pA in the absence and presence of rimonabant, respectively; n=5, p=0.03; Fig. 6D).

As Fig.6 shows the structural analog of rimonabant AM251, acting as CB1 antagonist and inverse agonist at low and high concentrations, respectively, prevented baclofen-induced outward current (20 μM: 55.2 ± 19.2 pA, n=5; p= 0.0018; Fig. 6F) in a dose-dependent fashion (2 μM: 117.5 ± 21.5 pA, n=6E; p= 0.14; Fig. 6E).

3.3 Rimonabant inhibits GTPγS induced GIRK channel gating—To evaluate whether rimonabant blocked GIRK activation by directly acting at the G protein, whole-cell patch-clamp recordings were performed in CHO cells transfected with GIRK1/2. GIRK currents were activated in a receptor-independent manner by GTPγS perfused into the cell via the recording pipette (Fig. 7A). GTPγS, exchanged for GDP at the Gα

subunit constitutively activates the G protein and leads to Gβγ subunit release that, in turn, activates GIRK channels (Logothetis et al., 1987). In the absence of rimonabant, GTPγS-induced inwardly rectifying K^+ currents that reached their peaks within 2 to 3 minutes of recording and exhibited modest desensitization over the 10 min recording period (Fig. 7AB). Rimonabant (10 μM) significantly prolonged the rise time of K^+ currents and reduced their maximal amplitudes (Fig. 7AB). These observations are consistent with rimonabant inhibiting G protein signaling and suggest a direct interaction of rimonabant with G protein subunits.

3.4 Rimonabant induces conformational changes in the heterotrimeric G protein—To investigate whether rimonabant induced BRET changes within the heterotrimeric G protein in the absence of receptors, we used HEK-293 cells transfected with $G\alpha_{i1}$ tagged with Venus and $G\beta_1$ or $G\gamma_2$ tagged with RLuc. The RLuc tag was inserted at the C-terminus of $G\beta_1$ or $G\gamma_2$ (Fig. 8A), where it does not affect the function of the Gβγ dimer (Gales et al., 2006). We used several $G\alpha_{i1}$ constructs, with Venus tags inserted into connecting loops at opposite ends of the helical domains (Fig. 8A). Venus was inserted into the loop connecting helices A and B ($G\alpha_{i1}$-91Venus) or in the loop connecting helices B and C ($G\alpha_{i1}$-121Venus). Venus was also introduced into the linker 1 region connecting the α-helical and the GTPase domain of $G\alpha_{i1}$ ($G\alpha_{i1}$-60Venus). Inserting Venus in these positions has been shown to affect neither the biochemical and catalytic properties of $G\alpha_{i1}$, nor the correct expression of and the efficient coupling of these fusion proteins to receptors (Gales et al., 2006; Ayoub et al., 2009). BRET was monitored between each tagged $G\alpha_{i1}$ ($G\alpha_{i1}$-60Venus, $G\alpha_{i1}$-91Venus and $G\alpha_{i1}$-121Venus) and $G\beta_1$-RLuc or $G\gamma_2$-RLuc. As shown in Fig. 8B, rimonabant significantly increased the basal BRET signal between $G\beta_1$-RLuc or $G\gamma_2$-RLuc and $G\alpha_{i1}$-91Venus, and between $G\beta_1$-RLuc or $G\gamma_2$-RLuc and $G\alpha_{i1}$-121Venus (Fig. 8C). No BRET change was detected between $G\alpha_{i1}$-60Venus and $G\beta_1$-Rluc or $G\gamma_2$-Rluc in the presence of rimonabant (25 μM) (Fig. 8D). The BRET changes monitored when using $G\alpha_{i1}$-91Venus and $G\alpha_{i1}$-121Venus as BRET acceptors probably reflect a rimonabant-promoted conformational rearrangement within the Gαβγ complex that may be differentially monitored depending on the position of the acceptor and donor.

4. DISCUSSION

At nanomolar concentrations, rimonabant inhibition of basal [^{35}S]GTPγS binding was interpreted either as an inverse agonism at CB1 receptors, i.e. the inhibition of constitutive CB1 receptor activity or the suppression of a tonic CB1 mediated activation of G protein by endogenous cannabinoids (Howlett et al., 2011; Pertwee 2005 for reviews). Inverse agonist effect induced by nanomolar concentrations has been observed in peculiar cell preparations expressing high concentration of the CB1 receptors (Lansdsman et al., 1997; MacLennan et al., 1998). However, under our experimental conditions, up to 100 nanomolar

concentrations of rimonabant failed to inhibit basal G protein activity. These discrepancies might be attributed to the different membranes preparations (i.e. neuroblastoma cells and CHO cells highly expressing CB1 receptors versus rodent brain tissues or untransfected CHO) and/or different buffer and ionic conditions used.

On the other hand, numerous studies indicated that rimonabant at micromolar concentration reliably reduces GTPγS binding in membrane from rodent, human and heterologous preparations in the presence or absence of CB1 receptors (Breivogel et al., 2001; Sim-Selley et al., 2001; Erdozain et al., 2012) and in CHO transfected with different GPCRs (Cinar and Szücs 2009; Zador et al., 2014, 2015).

It has been proposed that at micromolar concentrations rimonabant acts as inverse agonist at a putative GPCR receptor for which it has much lower affinity than for CB1 receptors (Breivogel et al., 2001; Cinar and Szücs 2009; Erdozain et al., 2012), or that might antagonize a tonic activation of the G protein by some endogenous ligand of a GPCR. Accordingly, Savinainem et al. (2003) postulated that rimonabant and AM251 reduce GTPγS binding by suppressing a tonic adenosine receptor mediated G-protein activation by endogenous adenosine. They based their hypothesis on the finding that in rat cerebellar membranes rimonabant and AM251 inhibited adenosine receptors and reduced GTPγS binding similarly to all other adenosine receptor antagonists tested. Moreover, neither rimonabant nor AM251 produced additional reduction of GTPγS beyond that induced by the specific A1 adenosine receptor DPCX. However, it should be pointed out that inhibitory effect of DPCX in cerebellar membranes was not reproduced by Erdozain et al (2012) in human cortical membranes. On the other hand different studies found that rimonabant and AM251 act as antagonists at opioid receptors (Cinar and Szücs 2009; Zador et al., 2014, 2015), suggesting that they may inhibit GTPγS binding by suppressing opioid receptor mediated G-protein activation by endogenous opioids.

The experiments outlined in this paper provide evidence that rimonabant causes a receptor-independent inhibition of $G\alpha_{i/o}$ activity, which uncouples the G protein from the receptor. Thus, in agreement with previous studies (Breivogel et al., 2001; Sim-Selley et al., 2001; Cinar and Szücs 2009; Zador et al., 2014), we found that rimonabant inhibited basal [^{35}S]GTPγS binding at concentrations of 4-5 μM, which are much higher than the nanomolar concentrations (0.5-1 nM) required to inhibit CB1 receptors (Rinaldi-Carmona et al., 1994). According to earlier work (Breivogel et al., 2001; Cinar and Szücs 2009; Erdozain et al., 2012) we demonstrated that rimonabant inhibited basal [^{35}S]GTPγS binding to cortical membranes of CB1-KO mice and untransfected CHO cells. Moreover, we found that rimonabant also decreased baclofen and quinpirole stimulated [^{35}S]GTPγS binding to cortical membranes of rats and CB1-KO mice. This inhibitory effect was not mediated by the action of rimonabant on CB1, $GABA_B$ or D2 receptors since it (i) persisted in CB1-KO mice and (ii) binds neither $GABA_B$ nor D2 receptors (Rinaldi-Carmona et al., 1994).

The efficacy of rimonabant in antagonizing baclofen- and quinpirole-induced stimulation of GTPγS binding was lower than expected by its efficacy in reducing basal GTPγS binding. It should be mentioned that rimonabant has been shown to inhibit [^{35}S]GTPγS binding to diverse G protein subunits with difference potency (Erdozain et al. 2012), suggesting that baclofen and quinpirole may act on a G-protein pool rather resistant to rimonabant inhibition. This possibility is consistent with the finding that 25 μM of rimonabant reduced both the potency and the efficacy of baclofen in stimulating GTPγS binding.

BRET data in living cells indicated that rimonabant stabilizes the heterotrimeric state of the G protein and prevents the rearrangement of $G\alpha_o$-βγ subunits induced by $GABA_B$ receptor activation. Rimonabant has lower potency in the BRET assay than in the GTPγS assay, possibly because the BRET assay is performed with intact cells.

Our results have shown that rimonabant inhibited GPCR-mediated activation of $G_{\alpha i/o}$ proteins and signaling to $G\alpha_{i/o}$ effectors. Indeed, rimonabant prevented agonist-induced inhibition of forskolin-stimulated cAMP production in HEK293 cells expressing $GABA_B$ or D2 receptors while it failed to inhibit $G\alpha_s$ mediated cAMP production in response to D1 receptor activation. Hence, rimonabant acts on the $G\alpha_{i/o}$ subunit of heterotrimeric G proteins. Future studies are required to evaluate whether or not rimonabant inhibits other G proteins, such as $G_{q/11}$ and G_{12}. Additionally, rimonabant suppressed baclofen and quinpirole-induced outward currents recorded from midbrain dopamine neurons of rats and CB1-KO mice as well as GIRK channel gating by GTPγS in CHO cells, confirming that it acts downstream and independently of GPCRs.

AM251, a structural analog of rimonabant, at micromolar concentrations decreased both the basal and the baclofen stimulated GTPγS binding to rat cortical membranes and to cell membranes of CHO cells stably expressing $GABA_B$ receptors. Moreover, AM251 dose-dependently prevented baclofen-induced outward currents recorded from midbrain dopamine neurons, suggesting that AM251 acts similarly to rimonabant at the same G-protein level.

Monitoring the BRET signal between probes inserted at various positions in the G protein subunits allows us to confirm that rimonabant promotes a receptor-independent conformational rearrangement within the Gαβγ complex, which is consistent with the stabilization of the heterotrimeric state. However, rimonabant failed to modify the BRET signal when $G\alpha_{i1}$ was mutated at position 60, thus suggesting a possible site of rimonabant action. Inserting the Venus tag into the linker 1 region of the $G\alpha_{i1}$ protein might disrupt this putative rimonabant binding site. The linker 1 region acts as a hinge during the opening of the α-helical domain, allowing GDP to leave the GTPase domain. Alternatively, and according to the "gear-shift" model (Cherfils et al., 2003), rimonabant might block the displacement of the α-helical domain away from the GTPase region by inhibiting the dissociation between the Gα subunit and the Gβγ

dimer, as indicated by the increase in the BRET signal between $G\beta_1$- or $G\gamma_2$- and $G\alpha_{i1}$-Venus (tagged in position 91 and 121).

Our results indicate that, at micromolar concentrations, rimonabant is not an inverse agonist of the CB1 receptor, as has been proposed (see Howlett et al., 2011; Pertwee 2005 for reviews), but inhibits the $G\alpha_{i/o}$ protein. The fact that rimonabant directly inhibits the $G\alpha_{i/o}$ protein is not alternative to the possibility that rimonabant may also act at the receptor level, which would contribute (e.g. opioid μ and δ and A1 adenosine receptor) (Cinar and Szücs 2009; Zador et al., 2014, 2015; Svinainem et al., 2003) to the inhibition of the G protein. Blocking of the G protein could, therefore, add to that of the CB1 receptor.

The inhibitory effect of micromolar concentrations of rimonabant on $G\alpha_{i/o}$ protein should be considered when interpreting its pharmacological effects. Indeed, the vast majority of *in vivo* experimental studies have used doses of rimonabant ranging from 1 to 10 mg/kg (Compton et al., 1996; Terranova et al., 1996; Gessa et al., 1998; Izzo et al., 1999a, 1999b; Pertwee 2001; Bass et al., 2002; Carai et al., 2004) which are expected to result in micromolar brain concentrations (ranging from 0.25 μM to 3 μM) (Barna et al., 2009; Tam et al., 2010). Regretfully, tissue and brain levels of rimonabant in clinical studies are not available. Rimonabant is a highly hydrophobic molecule with a long half-life (up to 16 days in obese subjects) that easily passes the blood brain barrier. It is therefore conceivable that it might reach micromolar tissue concentrations during a chronic daily treatment with 20-40 mg, which are the most effective doses in the treatment of obesity and nicotine addiction (Pi-Sunyer et al., 2006; Padwal and Majumdar 2007; Soyka et al., 2008; Cahill and Ussher 2011).

Since $Ga_{o/i}$ type G proteins are activated by multiple GPCRs, blockade of the G protein may be potentially useful in critical conditions, such as cancer and pain, characterized by the dysregulation of a number of GPCR signaling pathways (Ahmad and Dray 2004; Dorsam and Gutkind 2007), when targeting a single receptor is insufficient for effective treatment. For example, targeting the common $G\alpha_{i/o}$ protein could be therapeutically useful in the treatment of cancers that are characterized by elevated G protein activity (Smrcka 2013; Dorsam and Gutkind 2007). Consistently with this proposal, at low micromolar concentrations, rimonabant has been shown to exhibit cytotoxic and anti-proliferative effects with different cancer cells *in vitro*, including human lymphoma, human leukemia-derived cell lines, human breast cancer and glioma (Bifulco et al., 2007; Malfitano et al., 2007; Ciaglia et al., 2015). Remarkably, the antitumor effect has been shown to depend on the inhibition of a cascade of second messengers that are dependent on $G\alpha_{i/o}$-signaling (New et al., 2007; Ciaglia et al., 2015). However, more *in vivo* studies are needed to determine the toxicity of rimonabant doses inhibiting G protein signaling.

Conflicts of interest

The authors declare that they have no conflict of interests.

Acknowledgements

The authors would like to thank Dr. Martin Gaussman (Department of Biomedicine, University of Basel, Basel, Switzerland) for helpful discussions during revision.

Funding

This work was supported by a grant from the Fondazione Banco di Sardegna to MPC (U1005-2014/AI.887), and by grants from the National Center for Competences in Research (NCCR) 'Synapsy, Synaptic Bases of Mental Health Disease', the Swiss National Science Foundation (31003A-152970) and Sinergia (154411) to BB.

Authorship Contributions: MPC, GLG, and BB designed research; AP, MM, RT, CU performed research*;* AP, MM, RT, CU, IM analyzed data; MPC, GLG, BB and AP wrote the paper.

REFERENCES

Ahmad, S., Dray, A., 2004. Novel G protein-coupled receptors as pain targets. Curr. Opin. Investig. Drugs. 5, 67-70.

Ayoub, M.A., Damian, M., Gespach, C., Ferrandis, E., Lavergne, O., De Wever, O., Banères, J.L., Pin, J.P., Prévost, G.P., 2009. Inhibition of heterotrimeric G protein signaling by a small molecule acting on Galpha subunit. J. Bio. Chem. 284, 29136-29145.

Barna, I., Till, I., Haller, J., 2009. Blood, adipose tissue and brain levels of the cannabinoid ligands WIN 55,212 and SR-141716A after their intraperitoneal injection in mice: compound-specific and area-specific distribution within the brain. Eur. Neuropsychopharmacol. 19, 533-541.

Bass, C.E., Griffin, G., Grier, M., Mahadevan, A., Razdan, R.K., Martin, B.R., 2002. SR-141716A-induced stimulation of locomotor activity. A structure-activity relationship study. Pharmacol. Biochem. Behav. 74, 31-40.

Beardsley, P.M., Thomas, B.F., McMahon, L.R., 2009. Cannabinoid CB1 receptor antagonists as potential pharmacotherapies for drug abuse disorders. Int. Rev. Psychiatry 2, 134-142

Bifulco, M., Grimaldi, C., Gazzerro, P., Pisanti, S., Santoro, A., 2007. Rimonabant: just an antiobesity drug? Current evidence on its pleiotropic effects. Mol. Pharmacol. 71, 1445-1456

Bonacci, T.M., Mathews, J.L., Yuan, C., Lehmann, D.M., Malik, S., Wu, D., Font, J.L., Bidlack, J.M., Smrcka, A.V., 2006. Differential targeting of Gbetagamma-subunit signaling with small molecules. Science 312, 443-446.

Breivogel, C.S., Griffin, G., Di Marzo, V., Martin, B.R., 2001. Evidence for a new G protein-coupled cannabinoid receptor in mouse brain. Mol. Pharmacol. 60, 155-163.

Cahill, K., Ussher, M.H., 2011. Cannabinoid type 1 receptor antagonists for smoking cessation. Cochrane Database Syst. Rev. 16, CD005353

Carai, M.A., Colombo, G., Gessa, G.L., 2004. Rapid tolerance to the intestinal prokinetic effect of cannabinoid CB1 receptor antagonist, SR 141716 (Rimonabant). Eur. J. Pharmacol. 494, 221-224.

Castelli, M.P., Casu, A., Casti, P., Lobina, C., Carai, M.A., Colombo, G., Solinas, M., Giunta, D., Mugnaini, C., Pasquini, S., Tafi, A., Brogi, S., Gessa, G.L., Corelli F., 2012. Characterization of COR627 and COR628, two novel positive allosteric modulators of the GABA(B) receptor. J. Pharmacol. Exp. Ther. 340, 529-538.

Cherfils, J., Chabre, M., 2003. Activation of G-protein Galpha subunits by receptors through Galpha-Gbeta and Galpha-Ggamma interactions. Trends Biochem. Sci. 28, 13-17.

Christensen, R., Kristensen, P.K., Bartels, E.M., Bliddal, H., Astrup, A., 2007. Efficacy and safety of the weight-loss drug rimonabant: a meta-analysis of randomised trials. Lancet 370, 1706-1713.

Ciaglia, E., Torelli, G., Pisanti, S., Picardi, P., D'Alessandro, A., Laezza, C. ,Malfitano, A.M., Fiore, D., Pagano Zottola, A.C., Proto, M.C., Catapano, G., Gazzerro, P., and Bifulco, M., 2015. Cannabinoid receptor CB1 regulates STAT3 activity and its expression dictates the responsiveness to SR141716 treatment in human glioma patients' cells. Oncotarget. 6, 15464-15481.

Cinar, R., Szücs, M., 2009. CB1 receptor-independent actions of SR141716 on G-protein signaling: coapplication with the mu-opioid agonist Tyr-D-Ala-Gly-(NMe)Phe-Gly-ol unmasks novel, pertussis

toxin-insensitive opioid signaling in mu-opioid receptor-Chinese hamster ovary cells. J. Pharmacol. Exp. Ther. 330, 567-74.

Compton, D.R., Aceto, M.D., Lowe, J., Martin, B.R., 1996. In vivo characterization of a specific cannabinoid receptor antagonist (SR141716A): inhibition of delta 9-tetrahydrocannabinol-induced responses and apparent agonist activity. J. Pharmacol. Exp. Ther. 277, 586-94.

Denis, C., Saulière, A., Galandrin, S., Sénard, J.M., Galés, C., 2012. Probing heterotrimeric G protein activation: applications to biased ligands. Curr. Pharm. Des. 18, 128-144.

Dorsam, R.T., Gutkind, J.S., 2007. G-protein-coupled receptors and cancer. Nat. Rev. Cancer. 7, 79-94.

Erdozain, A.M., Diez-Alarcia, R., Meana, J.J., Callado, L.F., 2012. The inverse agonist effect of rimonabant on G protein activation is not mediated by the cannabinoid CB1 receptor: evidence from postmortem human brain. Biochem. Pharmacol. 83, 260-268.

Favre-Guilmard, C., Zeroual-Hider, H., Soulard, C., Touvay, C., Chabrier, P.E., Prevost, G., Auguet, M., 2008. The novel inhibitor of the heterotrimeric G-protein complex, BIM-46187, elicits anti-hyperalgesic properties and synergizes with morphine. Eur. J. Pharmacol. 594, 70-76.

Flygare, J., Gustafsson, K., Kimby, E., Christensson, B., Sander, B., 2005. Cannabinoid receptor ligands mediate growth inhibition and cell death in mantle cell lymphoma. FEBS Lett. 579, 6885-6889.

Freissmuth, M., Boehm, S., Beindl, W., Nickel, P., Ijzerman, A.P., Hoheneggeret M., 1996. Suramin analogues as subtype-selective G protein inhibitors. Mol. Pharmacol. 49, 602-611.

Fritzius, T., Turecek, R., Seddik, R., Kobayashi, H,. Tiao, J., Rem, P.D., Metz, M., Kralikova, M., Bouvier, M., Gassmann, M., Bettler. B., 2016. KCTD hetero-oligomers confer unique kinetic properties on hippocampal $GABA_B$ receptor-induced K+-currents. J. Neurosci. 37, 1162-1175.

Gales, C., Van Durm, J.J., Schaak, S., Pontier, S., Percherancier, Y., Audet, M., Paris, H., Bouvier, M., 2006. Probing the activation-promoted structural rearrangements in preassembled receptor-G protein complexes. Nat. Struct. Mol. Biol. 13, 778-786.

Gessa, G.L., Casu, M.A., Carta, G., Mascia M.S., 1998. Cannabinoids decrease acetylcholine release in the medial-prefrontal cortex and hippocampus, reversal by SR 141716A. Eur. J. Pharmacol. 355, 119-124.

Howlett, A.C., Reggio, P.H., Childers, S.R., Hampson, R.E., Ulloa, N.M., and Deutsch, D.G., 2011. Endocannabinoid tone versus constitutive activity of cannabinoid receptors. Br. J. Pharmacol. 163, 1329-43.

Izzo, A.A., Mascolo, N., Borrelli, F., Capasso, F., 1999a. Defaecation, intestinal fluid accumulation and motility in rodents: implications of cannabinoid CB1 receptors. Naunyn. Schmiedebergs. Arch. Pharmacol. 359, 65-70.

Izzo, A.A., Mascolo, N., Pinto, L., Capasso, R., Capasso, F., 1999b. The role of cannabinoid receptors in intestinal motility, defaecation and diarrhoea in rats. Eur. J. Pharmacol. 384, 37-42.

Jiang, L.I., Collins, J., Davis, R., Lin, K.M., DeCamp, D., Roach, T., Hsueh, R., Rebres, R.A., Ross, E.M., Taussig, R., Fraser, I., Sternweis, P.C., 2007. Use of a cAMP BRET sensor to characterize a novel regulation of cAMP by the sphingosine 1-phosphate/G13 pathway. J. Biol. Chem. 282, 10576-10584.

Jiang, Z.G., Pessia, M.,North, R.A., 1993. Dopamine and baclofen inhibit the hyperpolarization-activated cation current in rat ventral tegmental neurones. J. Physiol. 462, 753-764.

Johnson, S.W., North, R.A., 1992. Two types of neuron in the rat ventral tegmental area and their synaptic inputs. J. Physiol. 450, 455– 468.

Kan, Z., Jaiswal, B.S., Stinson, J., Janakiraman, V., Bhatt, D., 2010. Diverse somatic mutation patterns and pathway alterations in human cancers. Nature 466, 869-873.

Kaupmann, K., Malitschek, B., Schuler, V., Heid, J., Froestl, W., Beck, P., Mosbacher, J., Bischoff, S., Kulik, A., Shigemoto, R., Karschin, A., Bettler B., 1998. $GABA_B$ receptor subtypes assemble into functional heteromeric complexes. Nature 396, 683–687.

Lacey, M.G., Mercuri, N.B., North, R.A., 1988. On the potassium conductance increase activated by $GABA_B$ and dopamine D2 receptors in rat substantia nigra neurones. J. Physiol. 401, 437-453.

Landsman, R.S., Burkey, T.H., Consroe, P., Roeske, W.R., Yamamura, H.I., 1997. SR141716A is an inverse agonist at the human cannabinoid CB1 receptor. Eur J Pharmacol. 3, 334: R1-2.

Le Foll, B., Forget, B., Aubin, H.J., Goldberg, S.R., 2008. Blocking cannabinoid CB1 receptors for the treatment of nicotine dependence: insights from pre-clinical and clinical studies. Addict. Biol. 13, 239-252.

Logothetis, D.E., Kurachi, Y., Galper, J., Neer, E.J., Clapham, D.E., 1987. The beta gamma subunits of GTP-binding proteins activate the muscarinic K^+ channel in heart. Nature 325, 321-326.

MacLennan SJ, Reynen PH, Kwan J, Bonhaus D.W., 1998 Evidence for inverse agonism of SR141716A at human recombinant cannabinoid CB1 and CB2 receptors. Br J Pharmacol. 124, 619-22.

Malfitano, A.M., Laezza, C., Galgani, M., Matarese, G., D'Alessandro, A., Gazzerro, P., Bifulco, M., 2007. The CB1 receptor antagonist rimonabant controls cell viability and ascitic tumour growth in mice. Pharmacol. Res. 65, 365-371.

Marsicano, G., Wotjak, C.T., Azad, S.C., Bisogno, T., Rammes, G., Cascio, M.G., Hermann, H., Tang, J., Hofmann, C., Zieglgänsberger, W., Di Marzo, V., Lutz, B., 2002. The endogenous cannabinoid system controls extinction of aversive memories. Nature 418, 530-534.

Melis, M., Carta, S., Fattore, L., Tolu, S., Yasar, S., Goldberg, S.R., Fratta, W., Maskos, U., Pistis, M., 2010. Peroxisome proliferator-activated receptors-alpha modulate dopamine cell activity through nicotinic receptors. Biol. Psychiatry. 68, 256-264.

Meschler, J.P., Kraichely, D.M., Wilken, G.H., Howlett, AC., 2000. Inverse agonist properties of N-(piperidin-1-yl)-5-(4-chlorophenyl)-1-(2, 4-dichlorophenyl)-4-methyl-1H-pyrazole-3-carboxamide HCl (SR141716A) and 1-(2-chlorophenyl)-4-cyano-5-(4-methoxyphenyl)-1H-pyrazole-3-carboxyl ic acid phenylamide (CP-272871) for the CB(1) cannabinoid receptor. Biochem. Pharmacol. 60, 1315-1323.

Milligan, G., Kostenis, E., 2006. Heterotrimeric G-proteins: a short history. Br. J. Pharmacol. S46-55

Moreira, F.A., Grieb, M., Lutz, B., 2009. Central side-effects of therapies based on CB1 cannabinoid receptor agonists and antagonists: focus on anxiety and depression. Best. Pract. Res. Clin. Endocrinol. Metab. 23, 133-144.

New, D.C., Wu, K., Kwok, A.W.S., Wong, Y.H., 2007. G-protein coupled receptor-induced AKT activity in cellular proliferation and apoptosis. FEBS J. 274, 6025-6036.

Nishimura, A., Kitano, K., Takasaki, J., Taniguchi, M., Mizuno, N., Tago, K., Hakoshima, T., Itoh, H., 2010. Structural basis for the specific inhibition of heterotrimeric Gq protein by a small molecule. Proc. Natl. Acad. Sci. U.S.A. 107, 13666-13671.

Padwal, R.S., Majumdar, S.R., 2007. Drug treatments for obesity: orlistat, sibutramine, and rimonabant. Lancet 369, 71-77.

Pagano, A., Rovelli, G., Mosbacher, J., Lohmann, T., Duthey, B., Stauffer, D., Ristig, D., Schuler, V., Meigel, I., Lampert, C., Stein, T., Prezeau, L., Blahos, J., Pin, J., Froestl, W., Kuhn, R., Heid, J., Kaupmann, K., Bettler, B., 2001. C-terminal interaction is essential for surface trafficking but not for heteromeric assembly of GABA(b) receptors. J. Neurosci. 21, 1189-1202.

Pertwee, R.G., 2001. Cannabinoids and the gastrointestinal tract. Gut. Review. 48, 859-867.

Pertwee, R.G., 2005. Inverse agonism and neutral antagonism at cannabinoid CB1 receptors. Life Sci. 76, 1307-1324.

Pi-Sunyer, F.X., Aronne, L.J., Heshmati, H.M., Devin, J., Rosenstock, J., RIO-North America Study Group., 2006. Effect of rimonabant, a cannabinoid-1 receptor blocker, on weight and cardiometabolic risk factors in overweight or obese patients: RIO-North America: a randomized controlled trial. JAMA 295, 761-775.

Porcu, A., Lobina, C., Giunta, D., Solinas, M., Mugnaini, C., Castelli, M.P., 2016. In vitro and in vivo pharmacological characterization of SSD114, a novel GABAB positive allosteric modulator. Eur. J. Pharmacol. 791, 115-123.

Prévost, G.P., Lonchampt, M.O., Holbeck, S., Attoub, S., Zaharevitz, D., Alley, M., Wright, J., Brezak, M.C., Coulomb, H., Savola, A., Huchet, M., Chaumeron, S., Nguyen, Q.D., Forgez, P., Bruyneel, E., Bracke, M., Ferrandis, E., Roubert, P., Demarquay, D., Gespach, C., Kasprzyk PG., 2006. Anticancer activity of BIM-46174, a new inhibitor of the heterotrimeric Galpha/Gbetagamma protein complex. Cancer Res. 66, 9227-9234.

Raffa, R. B., Ward, S.J., 2012. CB1-independent mechanisms of Δ^9-THCV, AM251 and SR141716 (rimonabant). J. Clin. Pharm. Ther. 37, 260-265.

Rinaldi-Carmona, M., Barth, F., Héaulme, M., Shire, D., Calandra, B., Congy, C., Martinez, S., Maruani, J., Néliat, G., Caput, D., Ferrara, P., Soubrié, P., Claude Brelière, J., Le Fur, G., 1994. SR141716A, a potent and selective antagonist of the brain cannabinoid receptor. FEBS Lett. 350, 240-244.

Roman, D.L., 2009. Identification of ligands targeting RGS proteins high-throughput screening and therapeutic potential. Prog. Mol. Biol. Transl. Sci. 86, 335-356.

Rucker, D., Padwal, R., Li, S.K., Curioni, C, Lau, D.C., 2007. Long term pharmacotherapy for obesity and overweight: updated meta-analysis. BMJ. 335, 1194-1199.

Savinainen, J.R., Saario, S.M., Niemi, R., Järvinen, T., Laitinen, J.T., 2003. An optimized approach to study endocannabinoid signaling: evidence against constitutive activity of rat brain adenosine A1 and cannabinoid CB1 receptors. Br J Pharmacol.140, :1451-1459

Sato, M., Blumer, J.B., Simon, V., Lanier, S.M., 2006. Accessory proteins for G proteins: partners in signaling. Annu. Rev.Pharmacol.Toxicol. 46, 151-187.

Scheen, A.J., Finer, N., Hollander, P., Jensen, M.D., Van Gaal, L.F., and RIO-Diabetes Study Group, 2006. Efficacy and tolerability of rimonabant in overweight or obese patients with type 2 diabetes: a randomised controlled study. Lancet 368, 1660-1672.

Schuler, V., Lüscher, C., Blanchet, C., Klix, N., Sansig, G., Klebs, K., Schmutz, M., Heid, J., Gentry, C., Urban, L., Fox, A., Spooren, W., Jaton, A.L., Vigouret, J., Pozza, M., Kelly, P.H., Mosbacher, J., Froestl, W., Käslin, E., Korn, R., Bischoff, S., Kaupmann, K., van der Putten, H., Bettler, B., 2001. Epilepsy,

hyperalgesia, impaired memory, and loss of pre- and postsynaptic GABA(B) responses in mice lacking GABA(B(1)). Neuron 31, 47-58.

Sim-Selley, L.J., Brunk, L.K., Selley, D.E., 2001. Inhibitory effects of SR141716A on G-protein activation in rat brain. Eur. J. Pharmacol. 414, 135-143.

Sjögren, B., Blazer, L.L., Neubig, R.R., 2010. Regulators of G protein signaling proteins as targets for drug discovery. Prog. Mol. Biol. Transl. Sci. 91, 81-119.

Sjögren, B., 2011. Regulator of G protein signaling proteins as drug targets: current state and future possibilities. Adv. Pharmacol. 62, 315-347.

Smrcka, A.V., 2013. Molecular targeting of Gα and Gβγ subunits: a potential approach for cancer therapeutics. Trends Pharmacol. Sci. 34, 290-298.

Soyka, M., Koller, G., Schmidt, P., Lesch, O.M., Leweke, M., Fehr, C., Gann, H., Mann, K.F., 2008. Cannabinoid receptor 1 blocker rimonabant (SR 141716) for treatment of alcohol dependence: results from a placebo-controlled, double-blind trial. J. Clin. Psychopharmacol. 28, 317-324.

Syrovatkina, V., Alegre, K.O., Dey, R., Huang, X.Y., 2016. Regulation, Signaling, and Physiological Functions of G-Proteins. J. Mol. Biol. pii:S0022-2836.

Takasaki, J., Saito, T., Taniguchi, M., Kawasaki, T., Moritani, Y., Hayashi, K., Kobori, M. 2004. A novel Galphaq/11-selective inhibitor. J. Biol. Chem. 279, 47438-47445.

Tam, J., Vemuri, V.K., Liu, J., Bátkai, S., Mukhopadhyay, B., Godlewski, G., Osei-Hyiaman, D., Ohnuma, S., Ambudkar, S.V., Pickel, J., Makriyannis, A., Kunos, G., 2010. Peripheral CB1 cannabinoid receptor blockade improves cardiometabolic risk in mouse models of obesity. J. Clin. Invest. 120, 2953-2966.

Terranova, J.P., Storme, J.J., Lafon, N., Péfio, A., Rinaldi-Carmona, M., Le Fur, G., Soubrié, P., 1996. Improvement of memory in rodents by the selective CB1 cannabinoid receptor antagonist, SR 141716. Psychopharmac. (Berl) 126, 165-172.

Turecek, R., Schwenk, J., Fritzius, T., Ivankova, K., Zolles, G., Adelfinger, L., Jacquier, V., Besseyrias, V., Gassmann, M., Schulte, U., Fakler, B., Bettler, B., 2014. Auxiliary $GABA_B$ receptor subunits uncouple G protein βγ subunits from effector channels to induce desensitization. Neuron 82, 1032-1044.

Urwyler, S., Mosbacher, J., Lingenhoehl, K., Heid, J., Hofstetter, K., Froestl, W., Bettler, B., Kaupmann K., 2001. Positive allosteric modulation of native and recombinant gamma-aminobutyric acid(B) receptors by 2,6-Di-tert-butyl-4-(3-hydroxy-2,2-dimethyl-propyl)-phenol (CGP7930) and its aldehyde analog CGP13501. Mol. Pharm. 60, 963-971.

Van Gaal, L.F., Rissanen, A.M., Scheen, A.J., Ziegler, O., Rössner, S., RIO-Europe Study Group., 2005. Effects of the cannabinoid-1 receptor blocker rimonabant on weight reduction and cardiovascular risk factors in overweight patients: 1-year experience from the RIO-Europe study. Lancet 365, 1389-1397.

Vanhauwe, J.F., Fraeyman, N., Francken, B.J., Luyten, W.H., Leysen, J.E., 1999. Comparison of the ligand binding and signaling properties of human dopamine D(2) and D(3) receptors in Chinese hamster ovary cells. J. Pharmacol. Exp. Ther. 290, 908-916.

Xie, S., Furjanic, M.A., Ferrara, J.J., McAndrew, N.R., Ardino, E.L., Ngondara, A., Bernstein, Y., Thomas, K.J., Kim, E., Walker, J.M., Nagar, S., Ward, S.J., Raffa, R.B., 2007. The endocannabinoid system and rimonabant: a new drug with a novel mechanism of action involving cannabinoid CB1 receptor antagonism--or inverse agonism--as potential obesity treatment and other therapeutic use. J. Clin. Pharm. Ther. 32, 209-231.

Zádor, F., Kocsis, D., Borsodi, A., Benyhe, S., 2014. Micromolar concentrations of rimonabant directly inhibits delta opioid receptor specific ligand binding and agonist-induced G-protein activity. Neurochem. Int. 67,14-22.

Zádor, F., Lénárt, N., Csibrány, B., Sántha, M., Molnár, M., Tuka, B., Samavati, R., Klivényi, P., Vécsei, L., Marton, A., Vizler, C., Nagy, G.M., Borsodi, A., Benyhe, S., Páldy, E., 2015. Low dosage of rimonabant leads to anxiolytic-like behavior via inhibiting expression levels and G-protein activity of kappa opioid receptors in a cannabinoid receptor independent manner. Neuropharm. 89, 298-307.

FIGURE LEGENDS

FIGURE 1.Effect of rimonabant on agonist-stimulated G protein activity. Concentration-response curves for baclofen (BACL) were performed using [^{35}S]GTPγS binding assay in cortical membranes of rats (A) and of CB1-KO mice (B) in the presence of 5 μM rimonabant (RIM) or vehicle (VEH). (C) Concentration-response curves for quinpirole (QUINP) were performed using [^{35}S]GTPγS binding assays in rat striatal membranes in the presence of RIM or VEH. Data (A-C) are representative of a typical experiment performed in triplicate, and are expressed as percentage normalized to the respective basal value ± S.E.M. Non-visible S.E.M. is within the symbol.

FIGURE 2. Effects of rimonabant and AM251 on basal [^{35}S]GTPγS binding in rat frontal cortex membranes, in CHO-GABA$_B$ cell membranes and on baclofen-induced stimulation of [^{35}S]GTPγS binding in rat frontal cortex membranes. AM251 (AM) and rimonabant (RIM) at micromolar concentrations produce a significant inhibition of basal GTPγS binding both in membranes prepared from rat frontal cortex (A) and CHO-GABA$_B$ cells (B). Both compounds (C) significantly reduce the agonist effect induced by a submaximal concentration of baclofen (10 μM). Horizontal dotted lines indicate baseline values and the degree of stimulation with the agonist baclofen (BACL), respectively. Data, expressed as dpm, represent the mean ± SEM calculated from at least four independent experiments, each performed in triplicate **p<0.01, vs Basal and vs BACL 10 μM, Tukey test.

FIGURE 3. Rimonabant stabilized the heterotrimeric G$\alpha_{i/o}$ protein complex and prevented G protein rearrangements induced by the GABA$_B$ receptor agonist baclofen. (A) Illustration of the conformational change during G protein activation that is monitored by BRET measurements in CHO cells expressing GABA$_B$ receptors. Rluc probe in the Gα_o subunit is shown in blue and the Venus probe on the Gγ2 subunit is shown in yellow. (B) BRET kinetics measured in the presence of rimonabant (RIM) or the vehicle (VEH). Baclofen (BACL) (10 μM), applied after 29 cycles of reading (≈25 sec), decreased the BRET signal due to conformational rearrangement of the Gα_o-RLuc and Gγ2–Venus subunits. The curves were fitted with plateau followed by one-phase decay equation using Prism GraphPad software. The BRET ratio was calculated as the ratio of light emitted by Venus (530–570 nm) over the light emitted by RLuc (370–470 nm) and corrected by subtracting ratios obtained with the RLuc fusion protein alone. The results were expressed in mBRET units (BRET x 1000). Data points are presented as triplicates from one representative experiment. (C) Bar graph of the change in basal BRET is presented as mean ± SEM of 6 experiments. *p<0.05, **p<0.01, ***p<0.001,****p<0.0001 vs VEH, Bonferroni test. (D) Bar graph of the change in ΔBRET is presented as a mean ± SEM of 6 experiments. Horizontal dotted lines indicate

baseline values and the ΔBRET (%) values calculated in the presence of Baclofen *p<0.05, **p<0.01 vs BACL, Bonferroni test.

FIGURE 4. Effects of rimonabant on $GABA_B$ and D2 receptor signaling pathways: BRET kinetic measurements of cAMP responses using a CAMYEL sensor. (A) BRET signal (expressed as YFP/RLuc ratio), measured in the presence of rimonabant (RIM) or the vehicle (VEH) in HEK-293 cells transiently co-expressing the CAMYEL sensor and Myc-GABAB1a and Myc-GABAB2. 0.5 μM forskolin (FORSK) was applied after 150 seconds of reading, baclofen (BACL) 10 μM was applied after 500 seconds. The BRET recovery phases are shown fitted to a double exponential function (inset). Data points are presented as triplicates from one representative experiment. (B) Bar graph of the amplitude-weighted mean time constant (*tau* CAMYEL activity) was obtained by fitting BRET recovery phase to a double exponential function. Data are presented as mean ± SEM of 5 experiments. *p<0.05 and ***p<0.001 vs BACL alone, Bonferroni test. (C) Bar graph of the change in ΔBRET is presented as mean ± SEM of 5 experiments, performed in triplicate. **p<0.01, ***p<0.001 vs BACL alone, Bonferroni test. (D) BRET signal (expressed as YFP/RLuc ratio), measured in the presence of RIM or VEH in HEK-293 cells transiently co-expressing CAMYEL sensor and HA-D2. 0.5 μM forskolin was applied after 150 seconds of reading, quinpirole (QUINP) 10 μM was applied after 500 seconds. The BRET recovery phases are shown fitted to a double exponential function (inset). Data points are presented as triplicates from one representative experiment. (E) Bar graph of the amplitude-weighted mean time constant (*tau* CAMYEL activity) was obtained by fitting the BRET recovery phase to a double exponential function. Data are presented as mean ± SEM of 5 experiments. *p<0.05 vs QUINP alone, Bonferroni test. (F) Bar graph of the change in ΔBRET is presented as mean ± SEM of 5 experiments, performed in triplicate. Horizontal dotted lines indicate *tau* values and ΔBRET (%) values calculated in the presence of baclofen and quinpirole, respectively. **p<0.01, vs QUINP alone, Bonferroni test

FIGURE 5. Effects of rimonabant on D1 receptor signaling pathways: BRET kinetic measurements of cAMP responses using a CAMYEL sensor. (A) BRET signal (expressed as YFP/RLuc ratio), measured in the presence of rimonabant (RIM) or the vehicle (VEH) in HEK-293 cells transiently co-expressing the CAMYEL sensor and HA-D1. A68293 (10 μM) was applied after 25 seconds of reading. Data are presented as triplicates from one representative experiment. The curves were fitted with Plateau followed by one-phase decay equation using Prism GraphPad software. (B) Bar graph of the amplitude-weighted mean time constant (*tau* CAMYEL activity) was obtained by fitting the BRET recovery phase to a double exponential function. Data are presented as mean ± SEM of 5 experiments. (C) Bar graphs are calculated as the difference between the basal and the plateau of BRET signal. Horizontal dotted lines indicate *tau*

values and ΔBRET (%) values calculated in the presence of A68293. Data are the mean ± SEM of 5 experiments. ns= not significant, Bonferroni test.

FIGURE 6. Effect of rimonabant on K^+ currents evoked by $GABA_B$ and D2 receptor activation. Time course graphs illustrate the average effects of baclofen (10 μM, A-B-C), quinpirole (1 μM, D) and rimonabant (10 μM) on the holding current (I_{hold}) of dopamine cells *ex vivo*. When a voltage-clamped ($V_{holding}$= -70 mV) rat dopamine neuron is perfused with baclofen (BACL; 10 μM, gray bar) an outward current is evoked that is reproducible over time (A) unless rimonabant is applied (B; RIM; 10 μM, black bar). The inset in panel B shows that BACL (black line) caused a 132 pA outward current in voltage-clamp, which was abolished in the presence of RIM (RIM's effect on $I_{holding}$ is superimposed in light gray for comparison). The horizontal bar represents the time of BACL application. Calibration bar: 100 pA, 5 min. (C) RIM also prevents BACL-induced outward current in CB1-KO mouse dopamine neurons. (D) RIM blocks the outward current evoked upon activation of D2 receptors by quinpirole (QUINP; 1 μM, gray bar). (E, F) Effect of different concentrations of AM251 (AM), a structural analogue of rimonabant, on K^+ currents evoked by $GABA_B$ receptor activation. Time course graphs illustrate the average effects of BACL (10 μM, E and F) on the holding current (I_{hold}) of dopamine cells *ex vivo*. BACL (10 μM, gray bar) induces an outward current that is reproducible in the presence of a low concentration of AM (2 μM, AM 2) (E) but blunted at higher concentrations (20 μM, AM 20) (F). All data are normalized to the respective baseline current (5 min). Black bars show the time of superfusion of either VEH, RIM or AM. SEM bars are smaller than symbols in some cases. *p<0.05, **p<0.01, ***p<0.0001, paired *t*-test with Welch's correction.

FIGURE 7. Rimonabant slowed the onset of GTPγS-induced GIRK currents in CHO cells. (A) Representative traces of Kir3 currents activated by intracellular perfusion of GTPγS (0.6 mM) and recorded at -50 mV in transfected CHO cells expressing GIRK1/2 channels with 10 μM of RIM or with VEH. Note the slowly rising K^+ current in the presence of RIM. (B) Bar graph summarizing the densities (expressed as ratios between maximal amplitudes and the cell capacitances) and the 10% to 90% rise time of GTPγS-induced responses. Data are represented as mean ± SD of 5 VEH and 4 RIM recordings. **p < 0.01, ***p< 0.001; vs VEH; Student's t test.

FIGURE 8. Effect of rimonabant on $G\alpha_{i1}$-Gβγ subunits rearrangement in HEK-293 cells. (A) Schematic representation of the different tags on the G protein subunits. Rluc probes in Gβ1 and in the Gγ2 C-terminal are shown in blue and Venus probes on the $G\alpha_{i1}$ subunit are shown in yellow. BRET measurements in HEK-293 cells co-expressing Gβ1-RLuc or Gγ2-RLuc and either $G\alpha_{i1}$-91Venus (B), or

$G\alpha_{i1}$-121Venus (C) or $G\alpha_{i1}$-60Venus (D) subunits. The cells were incubated with RIM (rimonabant, 25 µM) (grey bars) or with the vehicle (black bars) for 1h at 37°C. Data are presented as a mean ± SEM of 5 experiments. *p<0.05, **p<0.01, ***p<0.0001 ns= not significant, Bonferroni test.

FIGURE SUPPL. 1 Effect of rimonabant on baclofen-stimulated [^{35}S]GTPγS binding in rat cortex membranes. At 25 µM rimonabant (RIM) inhibited the baclofen-stimulated GTPγS binding with an pEC50 of 3.79 (EC50 161 µM) and decreased its maximal (Emax ≈125). Data shown are representative of a typical experiment performed in triplicate, expressed as percentage normalized to the respective basal value ± S.E.M.

FIGURE SUPPL. 2

Normalized BRET ratio measured in the presence of rimonabant (RIM 50 µM) or vehicle (VEH). Baclofen (BACL) (10 µM), applied after 29 cycles of reading (≈25 sec), decreased the BRET signal due to a conformational rearrangement of the $G\alpha_o$-RLuc and Gγ2–Venus subunits. The curves were fitted with plateau followed by one-phase decay equation using Prism GraphPad software. The BRET ratio was calculated as the ratio of light emitted by Venus (530–570 nm) over the light emitted by RLuc (370–470 nm) and corrected by subtracting ratios obtained with the RLuc fusion protein alone. The data were expressed as BRET ratio and normalized to the baseline. Data points are presented as triplicates from one representative experiment. (B) Raw traces of the Rluc signal recorded at 370-470 nm, measured in the presence of increasing concentrations of rimonabant (RIM) or vehicle control (VEH) in CHO cells expressing $GABA_B$ receptors, Gαo-Rluc and Gγ2-HA. Injection of BACL (10 µM) produced similar injection artifacts in all traces. Data points from a representative experiment (n =3) are expressed as relative luminescence units (RLU).

TABLE 1

Rimonabant induced inhibition of basal [^{35}S]GTPγS binding in native and recombinant systems.

	IC_{50} (μM)	Maximal Inhibition (%)
Rat cortex	3.9 ± 0.4	48 ± 2.6
Rat striatum	3.7 ± 0.5	50 ± 3.3
CB1 KO mice (cortex)	12.1 ± 2.1	38 ± 1.5
WT littermate mice (cortex)	12.6 ± 2.1	36 ± 1.0
$GABA_B$ KO mice (cortex)	4.3 ± 1.2	50 ± 1.4
WT littermate mice (cortex)	3.9 ± 0.8	48 ± 1.7
CHO-$GABA_B$ cells	6.9 ± 1.1	27 ± 1.9
CHO-D2 cells	10.5 ± 4.6	24 ± 2.0
Parental CHO cells	7.6 ± 2.7	22 ± 1.7

Concentration response curves for rimonabant (RIM) were performed in native or in recombinant systems (Chinese Hamster Ovary, CHO cells). RIM decreased basal [^{35}S]GTPγS binding independently of the presence or absence of the GPCR. Data are expressed as percentage stimulation over basal [^{35}S]GTPγS binding, measured in the absence of RIM and defined as 100%, as described in material and methods. IC50 and Imax are calculated with GraphPad using non-linear regression analysis of the concentration-response curve performed in the brain or in CHO membrane preparation. Maximal RIM inhibition was expressed as the percentage of inhibition relative to 100%. WT: wild type

Table 2: **Rimonabant decreased $GABA_B$ and D2 receptor agonists-stimulated [^{35}S]GTPγS binding in rat, mouse cortical and striatal membranes.**

		EC50 (μM)	pEC50 (-Log M)	pEC50 (95% CI)	Maximal effect relative to BACL or QUINP (%)
Rat cortex	BACL	7.30 ± 1.10	5.15 ± 0.06	4.96-5.34	100.00 ± 5.06
Rat cortex	BACL +RIM	11.32 ±1.00*	4.91 ± 0.03*	4.84-5.06	94.48 ± 3.68
CB1-KO mice (cortex)	BACL	2.48 ± 0.64	5.65 ± 0.11	5.29-6.01	100.00 ± 3.08
CB1-KO mice (cortex)	BACL+ RIM	4.26 ± 0.17+	5.37 ± 0.02+	5.32-5.42	94.83 ± 3.27
Rat striatum	QUINP	3.36 ± 0.14	5.47 ± 0.02	5.39-5.55	100.00 ± 6.59
Rat striatum	QUINP + RIM	9.17 ± 1.85&	5.06 ± 0.09&	4.65-5.46	105.50 ± 4.49

The selective $GABA_B$ and D2 receptor agonists were tested alone or in combination with rimonabant (RIM) (5 μM). RIM decreased the potency of baclofen (BACL)- and quinpirole (QUINP)-stimulated [^{35}S]GTPγS binding in rat cortical and striatal membranes and in membranes of CB1-KO mice. RIM did not modify the maximal efficacy of agonists. Data are expressed as percentage stimulation over their respective baseline values and represent the mean ± SEM calculated from at least four independent experiments, each performed in triplicate. Data are fitted with the GraphPad Prism 6.0 software using nonlinear regression and sigmoidal curve fitting to obtain EC50, pEC50 and maximal effect values. As the maximal effect of BACL and QUINP alone differed between experiments, data are normalized to the maximal effect of BACL and QUINP under control conditions (=100). CI; values represent 95 % confidence intervals of values from four experiments; *$p < 0.05$ vs baclofen (Rat Cortex) ; +$p < 0.05$ vs baclofen (CB1-KO Mice), &$p < 0.05$ vs quinpirole (Rat Striatum); unpaired Student's *t*-test.

FIGURE 1

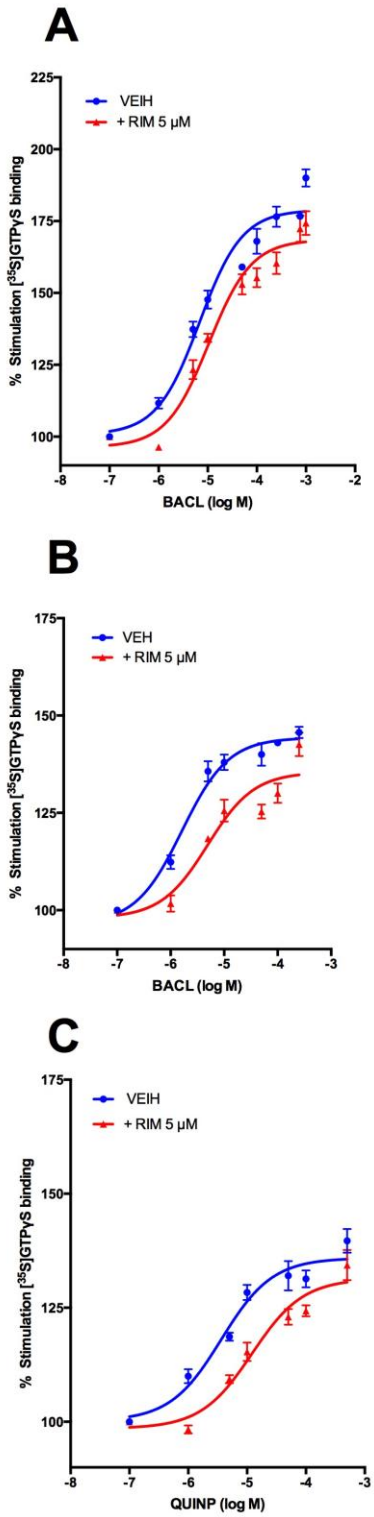
A
VEIH
+ RIM 5 µM
% Stimulation [35S]GTPγS binding
BACL (log M)
B
VEH
+ RIM 5 µM
% Stimulation [35S]GTPγS binding
BACL (log M)
C
VEIH
+ RIM 5 µM
% Stimulation [35S]GTPγS binding
QUINP (log M)

FIGURE 2

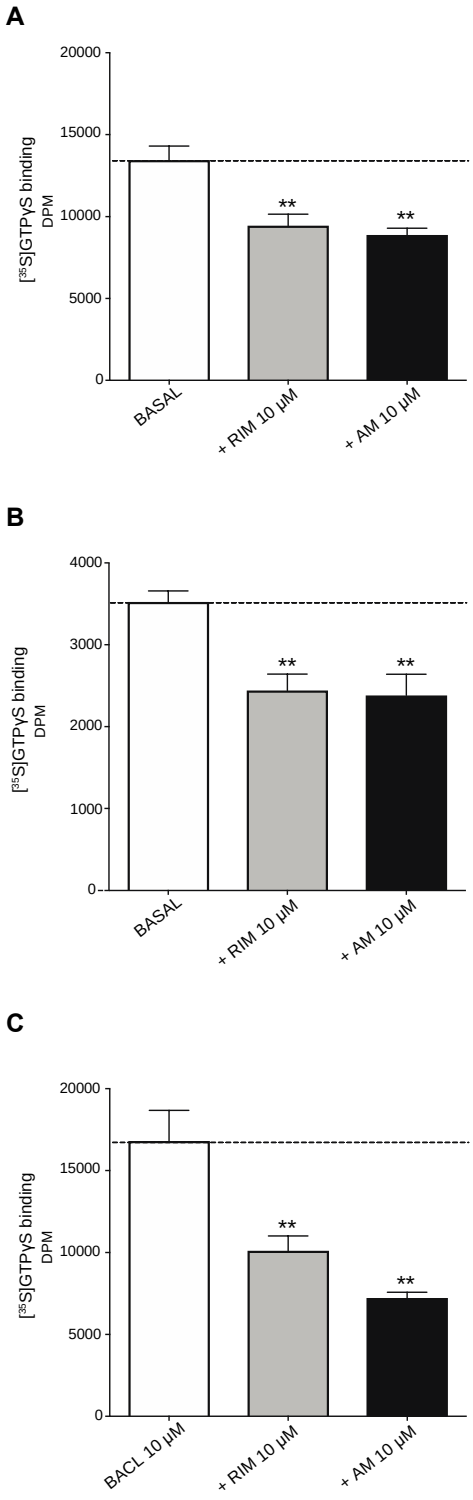
A
20000
15000
10000
5000
0
[35S]GTPγS binding
DPM
**
**
BASAL
+ RIM 10 μM
+ AM 10 μM
B
4000
3000
2000
1000
0
[35S]GTPγS binding
DPM
**
**
BASAL
+ RIM 10 μM
+ AM 10 μM
C
20000
15000
10000
5000
0
[35S]GTPγS binding
DPM
**
**
BACL 10 μM
+ RIM 10 μM
+ AM 10 μM

FIGURE 3

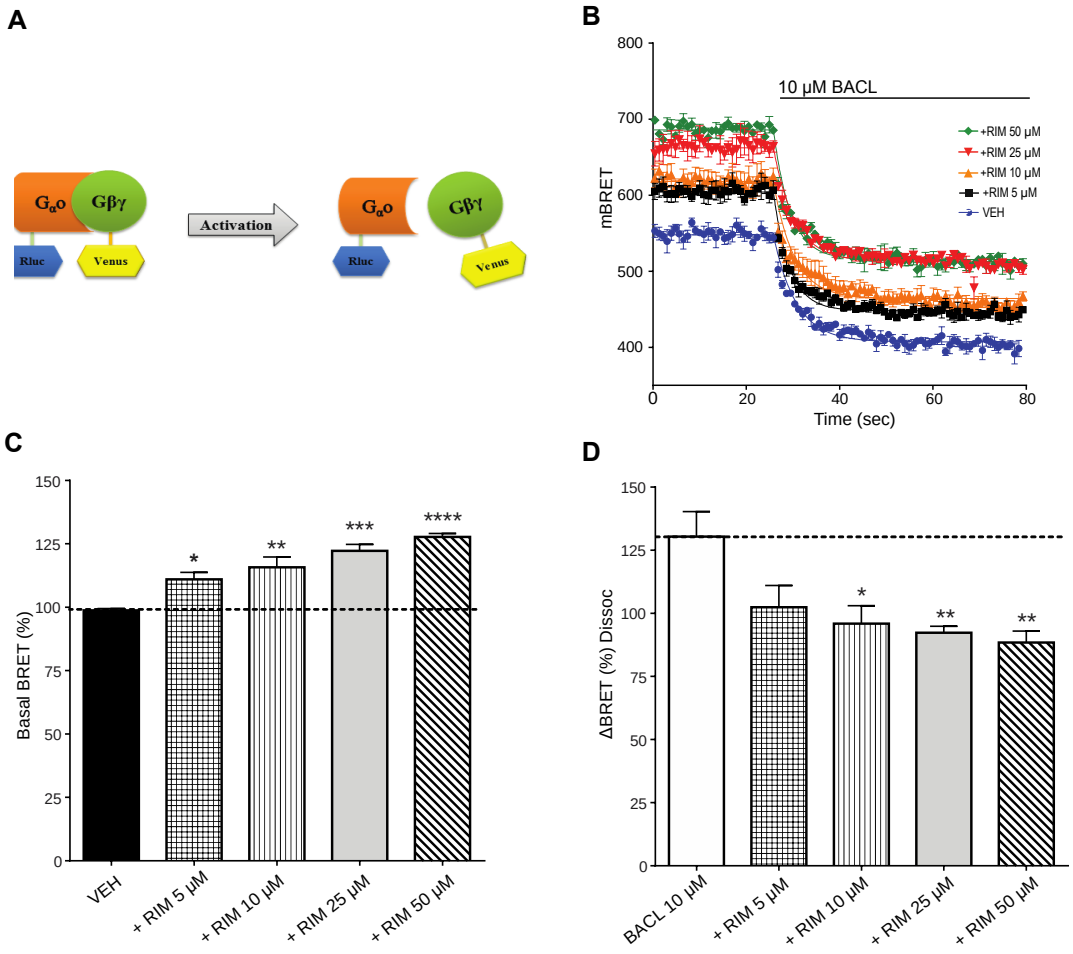
A
Gαo
Gβγ
Rluc
Venus
Activation
B
10 μM BACL
+RIM 50 μM
+RIM 25 μM
+RIM 10 μM
+RIM 5 μM
VEH
mBRET
Time (sec)
C
Basal BRET (%)
VEH
+ RIM 5 μM
+ RIM 10 μM
+ RIM 25 μM
+ RIM 50 μM
D
ΔBRET (%) Dissoc
BACL 10 μM
+ RIM 5 μM
+ RIM 10 μM
+ RIM 25 μM
+ RIM 50 μM

FIGURE 4

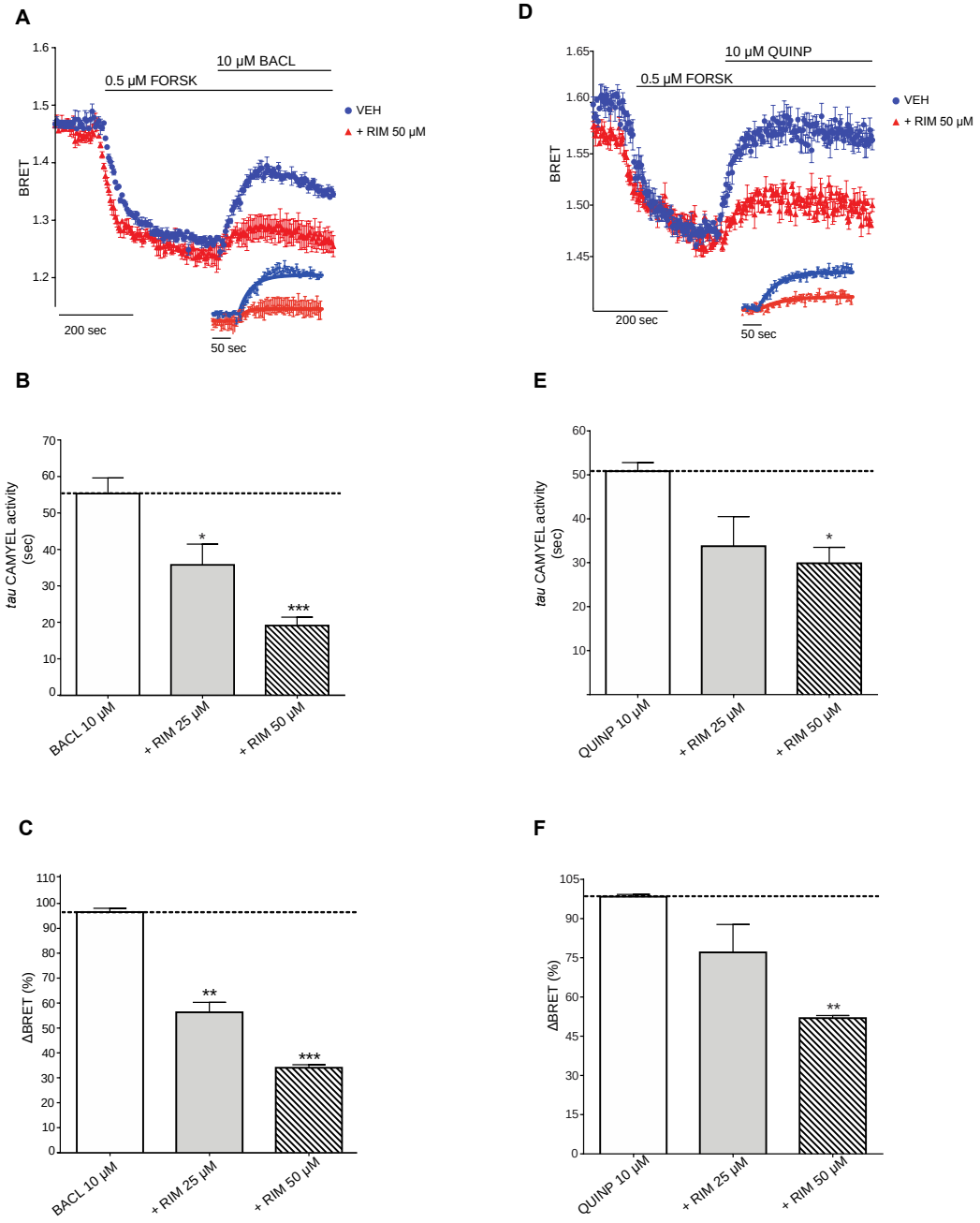
A
10 µM BACL
0.5 µM FORSK
VEH
+ RIM 50 µM
BRET
200 sec
50 sec
D
10 µM QUINP
0.5 µM FORSK
VEH
+ RIM 50 µM
BRET
200 sec
50 sec
B
tau CAMYEL activity (sec)
BACL 10 µM
+ RIM 25 µM
+ RIM 50 µM
E
tau CAMYEL activity (sec)
QUINP 10 µM
+ RIM 25 µM
+ RIM 50 µM
C
ΔBRET (%)
BACL 10 µM
+ RIM 25 µM
+ RIM 50 µM
F
ΔBRET (%)
QUINP 10 µM
+ RIM 25 µM
+ RIM 50 µM

FIGURE 5

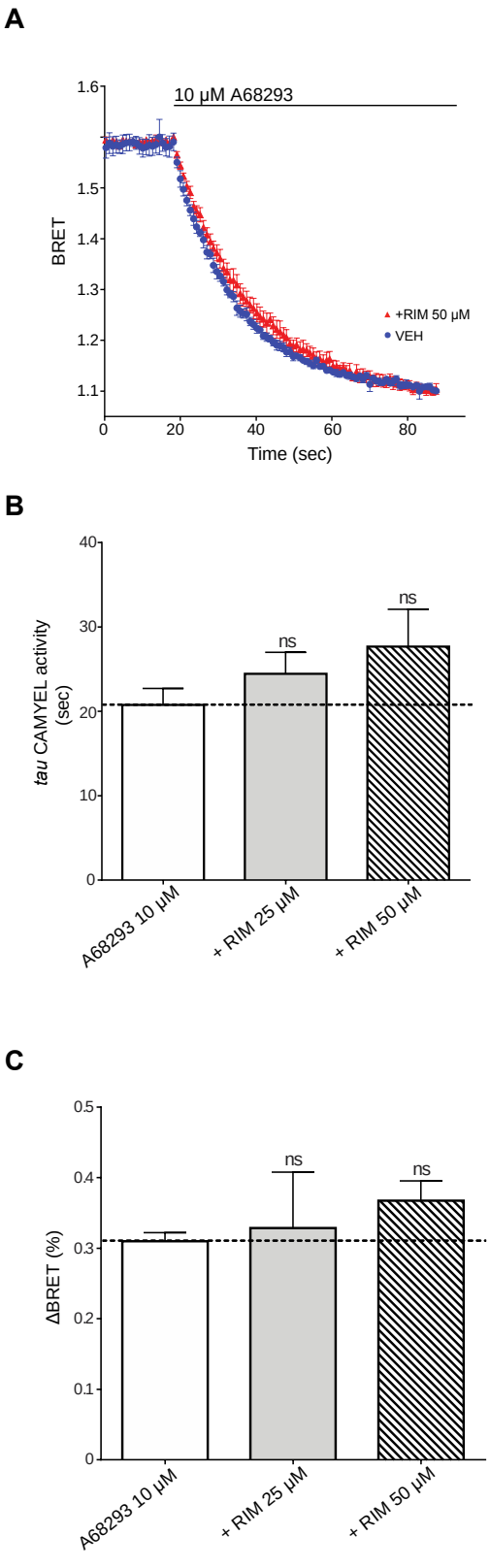
A
10 µM A68293
BRET
Time (sec)
+RIM 50 µM
VEH
B
tau CAMYEL activity (sec)
ns
ns
A68293 10 µM
+ RIM 25 µM
+ RIM 50 µM
C
ΔBRET (%)
ns
ns
A68293 10 µM
+ RIM 25 µM
+ RIM 50 µM

FIGURE 6

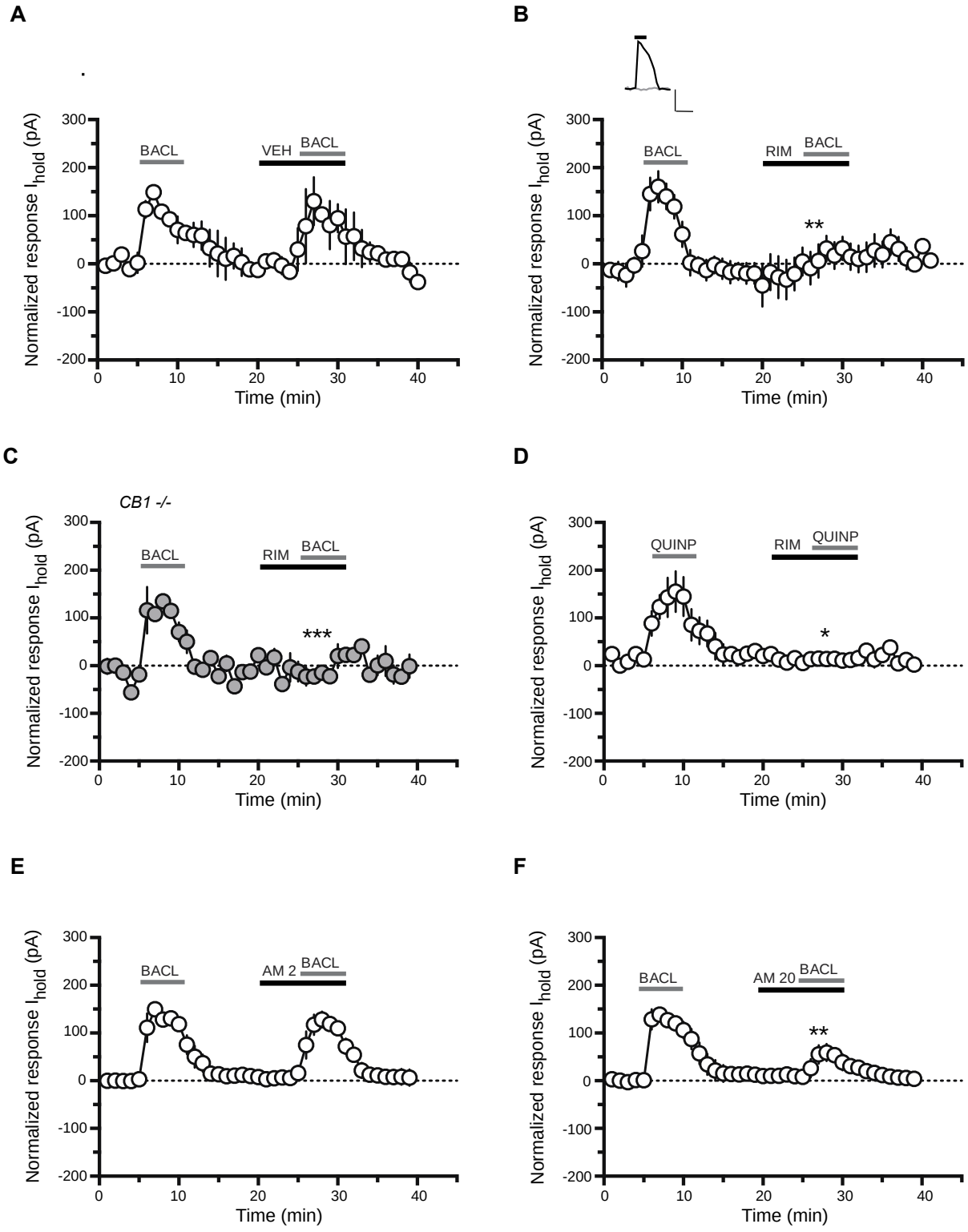
A
B
C
D
E
F
CB1 -/-
BACL
VEH
RIM
QUINP
AM 2
AM 20
Normalized response Ihold (pA)
Time (min)
*
**
***

FIGURE 7

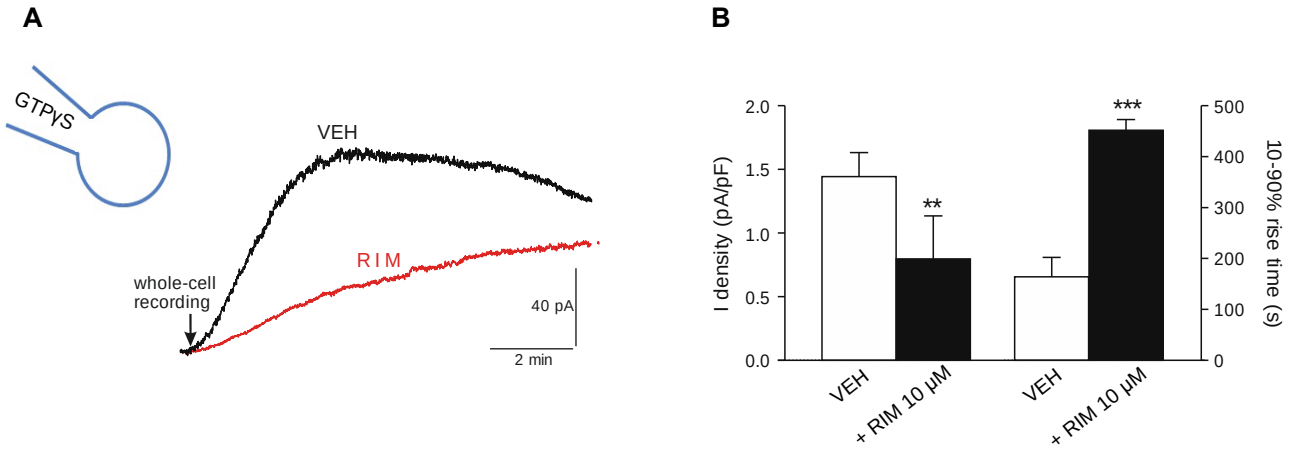
A
GTPγS
VEH
RIM
whole-cell
recording
40 pA
2 min
B
I density (pA/pF)
10-90% rise time (s)
2.0
1.5
1.0
0.5
0.0
500
400
300
200
100
0
**
***
VEH
+ RIM 10 μM
VEH
+ RIM 10 μM

FIGURE 8

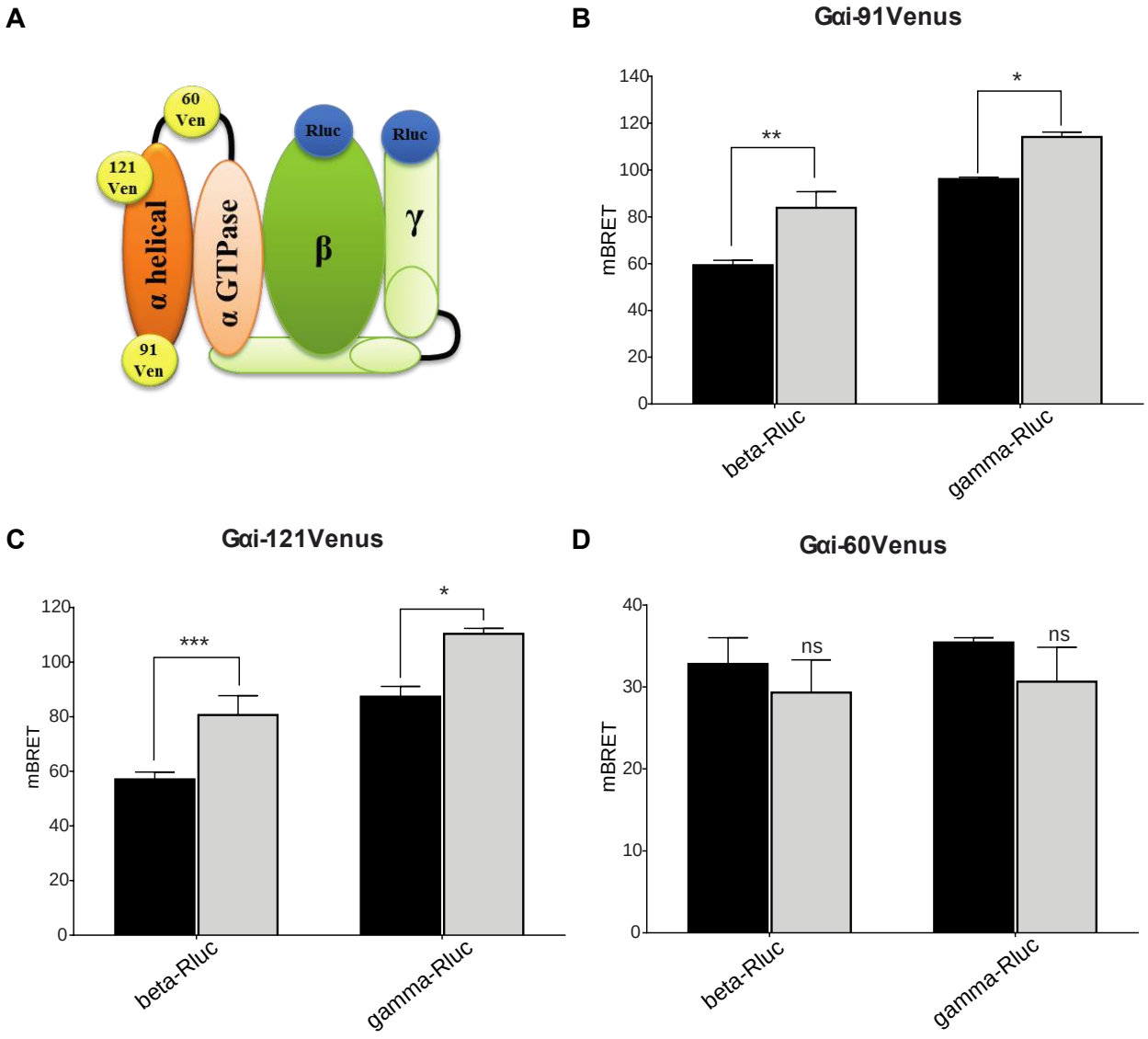
A
60 Ven
121 Ven
α helical
α GTPase
β
γ
Rluc
Rluc
91 Ven
B
Gαi-91Venus
mBRET
140
120
100
80
60
40
20
0
**
*
beta-Rluc
gamma-Rluc
C
Gαi-121Venus
mBRET
120
100
80
60
40
20
0
***
*
beta-Rluc
gamma-Rluc
D
Gαi-60Venus
mBRET
40
30
20
10
0
ns
ns
beta-Rluc
gamma-Rluc

FIGURE SUPPL. 1

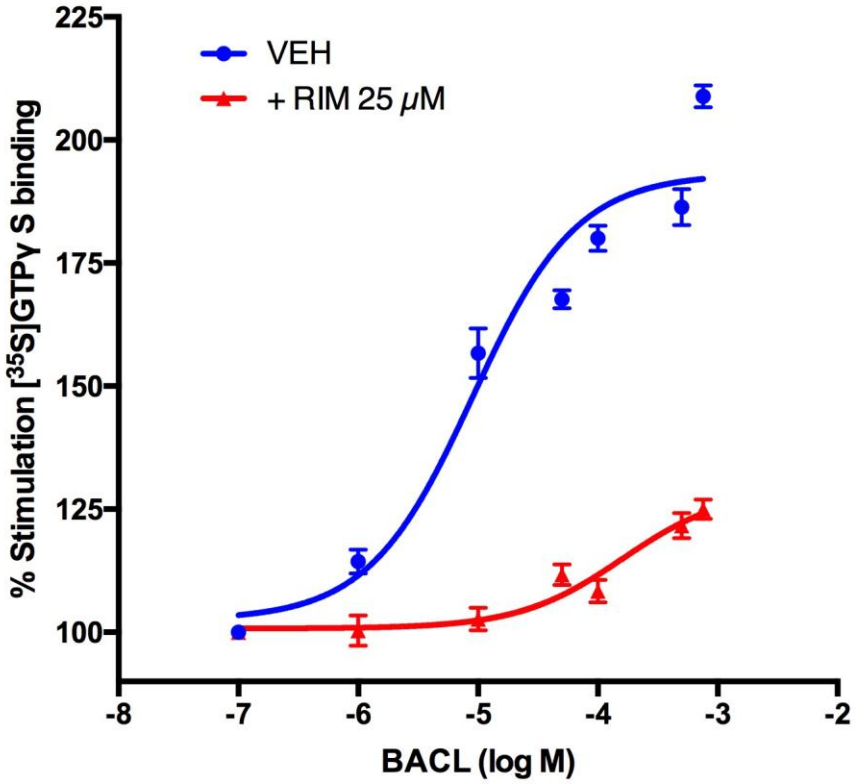

FIGURE SUPPL. 2.

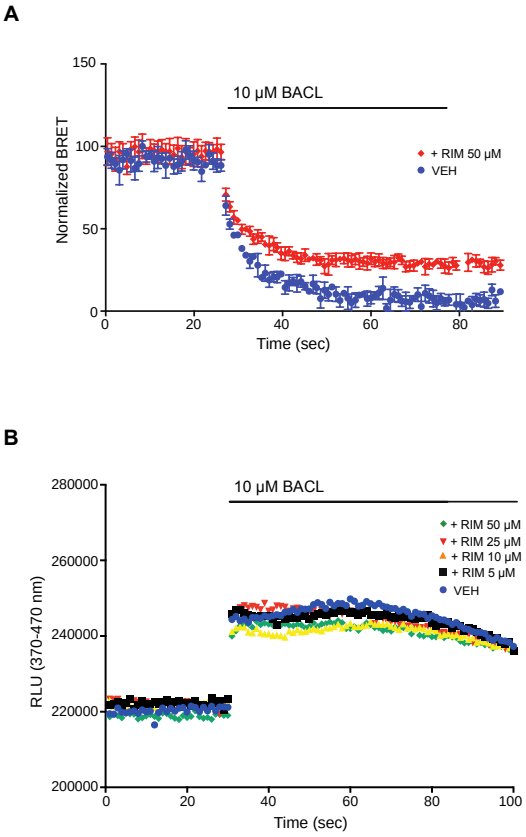

TABLE 1

Rimonabant induced inhibition of basal [^{35}S]GTPγS binding in native and recombinant systems.

	IC_{50} (μM)	Maximal Inhibition (%)
Rat cortex	3.9 ± 0.4	48 ± 2.6
Rat striatum	3.7 ± 0.5	50 ± 3.3
CB1 KO mice (cortex)	12.1 ± 2.1	38 ± 1.5
WT littermate mice (cortex)	12.6 ± 2.1	36 ± 1.0
$GABA_B$ KO mice (cortex)	4.3 ± 1.2	50 ± 1.4
WT littermate mice (cortex)	3.9 ± 0.8	48 ± 1.7
CHO-$GABA_B$ cells	6.9 ± 1.1	27 ± 1.9
CHO-D2 cells	10.5 ± 4.6	24 ± 2.0
Parental CHO cells	7.6 ± 2.7	22 ± 1.7

Concentration response curves for rimonabant (RIM) were performed in native or in recombinant systems (Chinese Hamster Ovary, CHO cells). RIM decreased basal [^{35}S]GTPγS binding independently of the presence or absence of the GPCR. Data are expressed as percentage stimulation over basal [^{35}S]GTPγS binding, measured in the absence of RIM and defined as 100%, as described in material and methods. IC50 and Imax are calculated with GraphPad using non-linear regression analysis of the concentration-response curve performed in the brain or in CHO membrane preparation. Maximal RIM inhibition was expressed as the percentage of inhibition relative to 100%. WT: wild type

Table 2

Table 2: **Rimonabant decreased $GABA_B$ and D2 receptor agonists-stimulated [^{35}S]GTPγS binding in rat, mouse cortical and striatal membranes.**

		EC50 (μM)	pEC50 (-Log M)	(95% CI)	Maximal effect relative to BACL or QUINP (%)
Rat cortex	BACL	7.30 ± 1.10	5.15 ± 0.06	4.96-5.34	100.00 ± 5.06
Rat cortex	BACL +RIM	11.32 ±1.00*	4.91 ± 0.03*	4.84-5.06	94.48 ± 3.68
CB1-KO mice (cortex)	BACL	2.48 ± 0.64	5.65 ± 0.11	5.29-6.01	100.00 ± 3.08
CB1-KO mice (cortex)	BACL+ RIM	4.26 ± 0.17^{+}	5.37 ± 0.02^{+}	5.32-5.42	94.83 ± 3.27
Rat striatum	QUINP	3.36 ± 0.14	5.47 ± 0.02	5.39-5.55	100.00 ± 6.59
Rat striatum	QUINP + RIM	9.17 ± 1.85$^{\&}$	5.06 ± 0.09$^{\&}$	4.65-5.46	105.50 ± 4.49

The selective $GABA_B$ and D2 receptor agonists were tested alone or in combination with rimonabant (RIM) (5 μM). RIM decreased the potency of baclofen (BACL)- and quinpirole (QUINP)-stimulated [^{35}S]GTPγS binding in rat cortical and striatal membranes and in membranes of CB1-KO mice. RIM did not modify the maximal efficacy of agonists. Data are expressed as percentage stimulation over their respective baseline values and represent the mean ± SEM calculated from at least four independent experiments, each performed in triplicate. Data are fitted with the GraphPad Prism 6.0 software using nonlinear regression and sigmoidal curve fitting to obtain EC50, pEC50 and maximal effect values. As the maximal effect of BACL and QUINP alone differed between experiments, data are normalized to the maximal effect of BACL and QUINP under control conditions (=100). CI; values represent 95 % confidence intervals of values from four experiments; *p < 0.05 vs baclofen (Rat Cortex); $^{+}$p < 0.05 vs baclofen (CB1-KO Mice), $^{\&}$p < 0.05 vs quinpirole (Rat Striatum); unpaired Student's *t*-test.

Figure 1

A

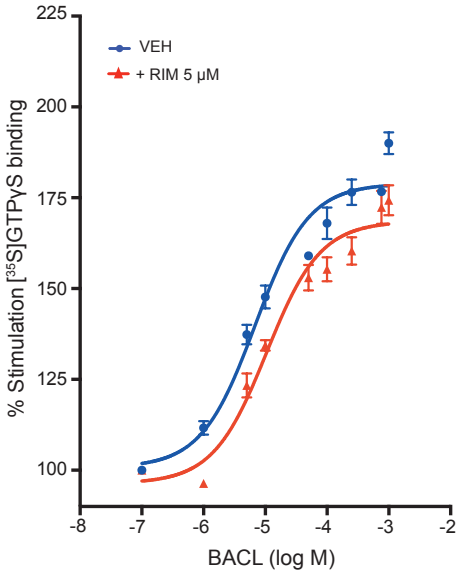
VEH
+ RIM 5 μM
% Stimulation [35S]GTPγS binding
225
200
175
150
125
100
-8
-7
-6
-5
-4
-3
-2
BACL (log M)

B

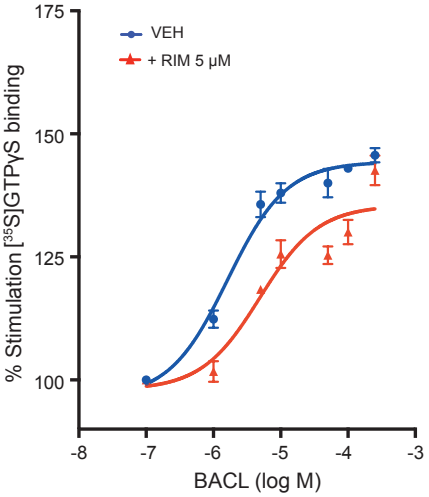
VEH
+ RIM 5 μM
% Stimulation [35S]GTPγS binding
175
150
125
100
-8
-7
-6
-5
-4
-3
BACL (log M)

C

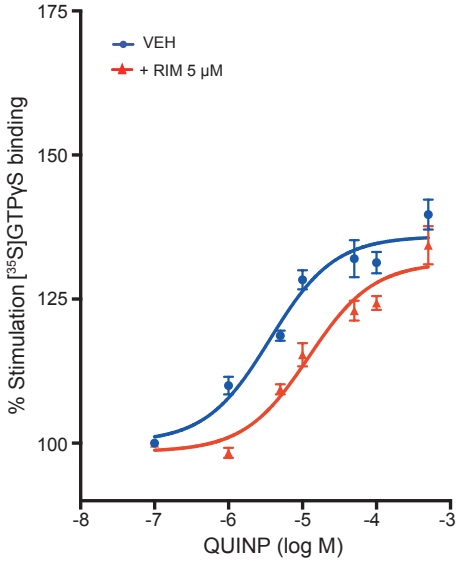
VEH
+ RIM 5 μM
% Stimulation [35S]GTPγS binding
175
150
125
100
-8
-7
-6
-5
-4
-3
QUINP (log M)

Figure 2

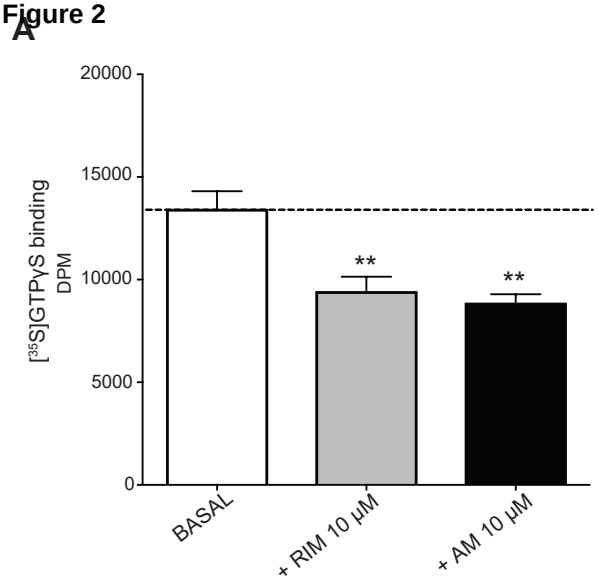
A
20000
15000
10000
5000
0
[35S]GTPγS binding
DPM
**
**
BASAL
+ RIM 10 μM
+ AM 10 μM

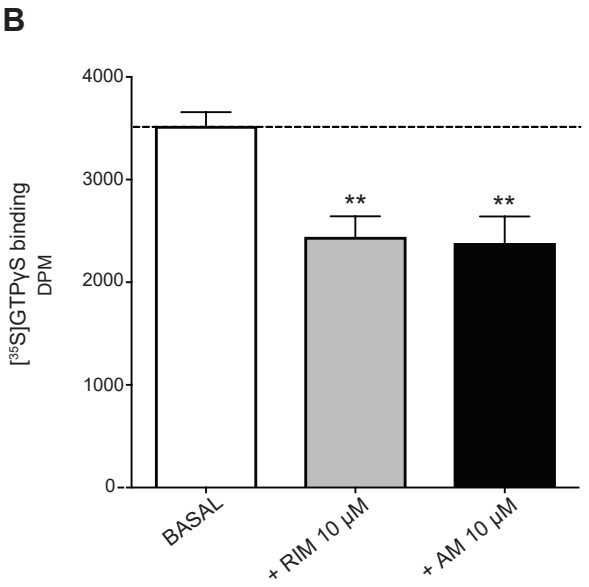
B
4000
3000
2000
1000
0
[35S]GTPγS binding
DPM
**
**
BASAL
+ RIM 10 μM
+ AM 10 μM

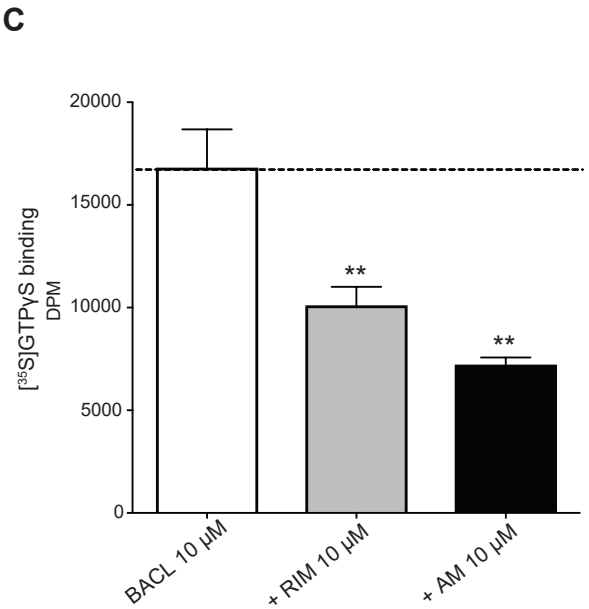
C
20000
15000
10000
5000
0
[35S]GTPγS binding
DPM
**
**
BACL 10 μM
+ RIM 10 μM
+ AM 10 μM

Figure 3
C

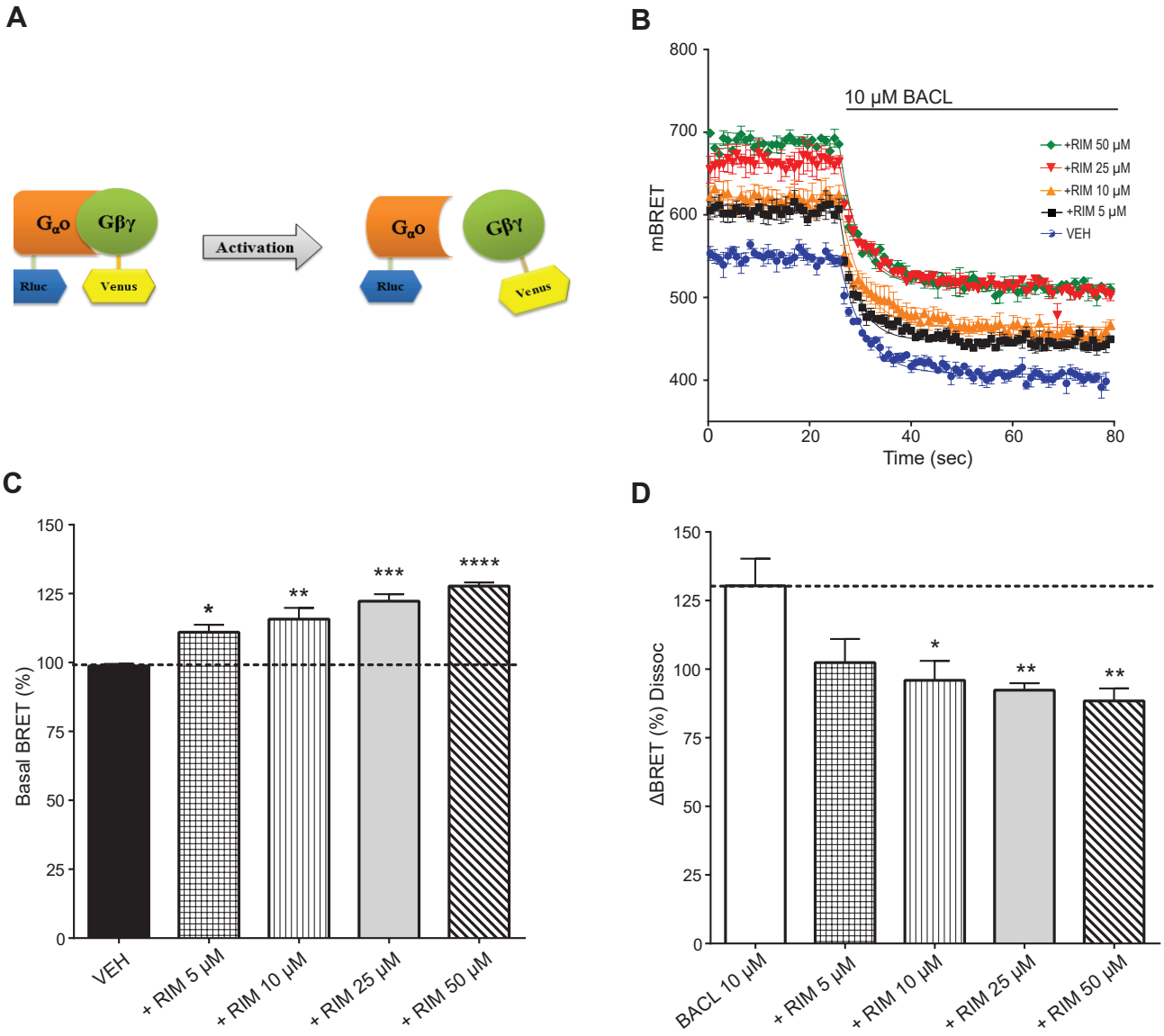
A
Gαo
Gβγ
Rluc
Venus
Activation
Gαo
Gβγ
Rluc
Venus
B
10 μM BACL
+RIM 50 μM
+RIM 25 μM
+RIM 10 μM
+RIM 5 μM
VEH
mBRET
Time (sec)
C
Basal BRET (%)
VEH
+ RIM 5 μM
+ RIM 10 μM
+ RIM 25 μM
+ RIM 50 μM
D
ΔBRET (%) Dissoc
BACL 10 μM
+ RIM 5 μM
+ RIM 10 μM
+ RIM 25 μM
+ RIM 50 μM

Figure 4

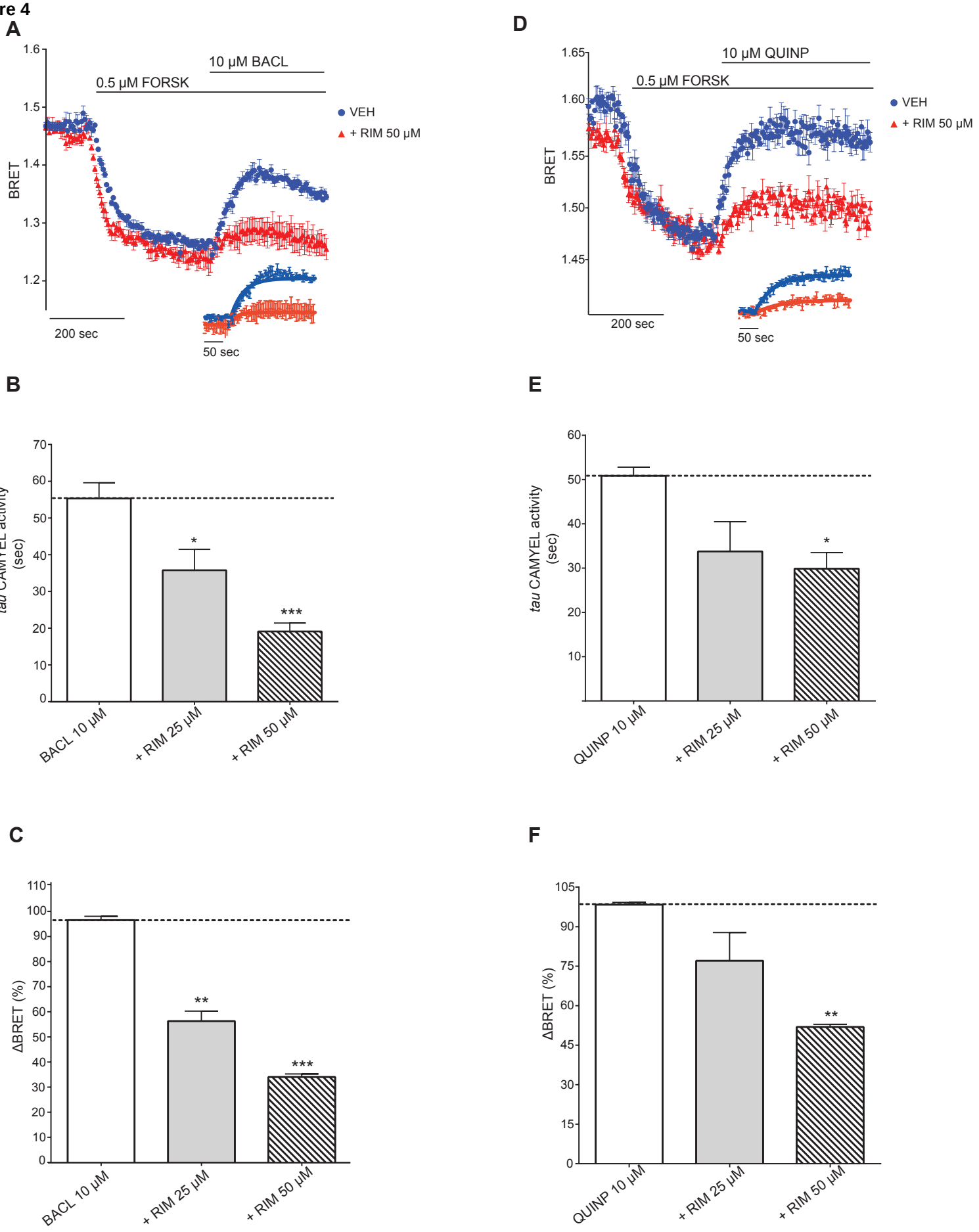
A
10 µM BACL
0.5 µM FORSK
VEH
+ RIM 50 µM
BRET
200 sec
50 sec
D
10 µM QUINP
0.5 µM FORSK
VEH
+ RIM 50 µM
BRET
200 sec
50 sec
B
tau CAMYEL activity (sec)
BACL 10 µM
+ RIM 25 µM
+ RIM 50 µM
E
tau CAMYEL activity (sec)
QUINP 10 µM
+ RIM 25 µM
+ RIM 50 µM
C
ΔBRET (%)
BACL 10 µM
+ RIM 25 µM
+ RIM 50 µM
F
ΔBRET (%)
QUINP 10 µM
+ RIM 25 µM
+ RIM 50 µM

Figure 5

A

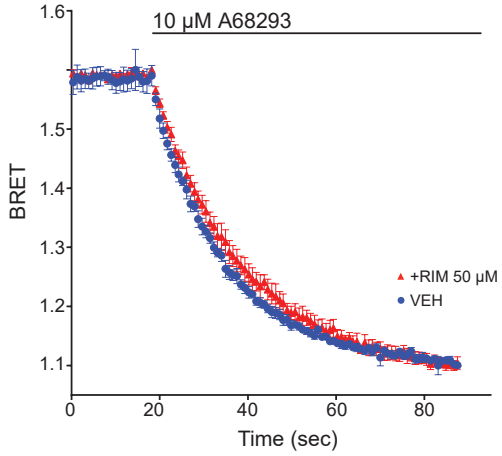
10 μM A68293
BRET
Time (sec)
+RIM 50 μM
VEH

B

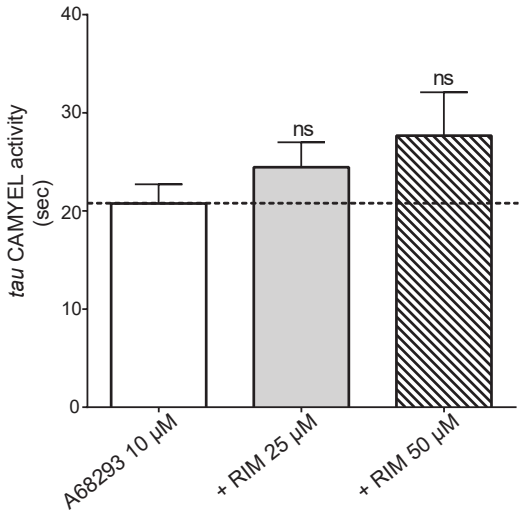
tau CAMYEL activity (sec)
ns
ns
A68293 10 μM
+ RIM 25 μM
+ RIM 50 μM

C

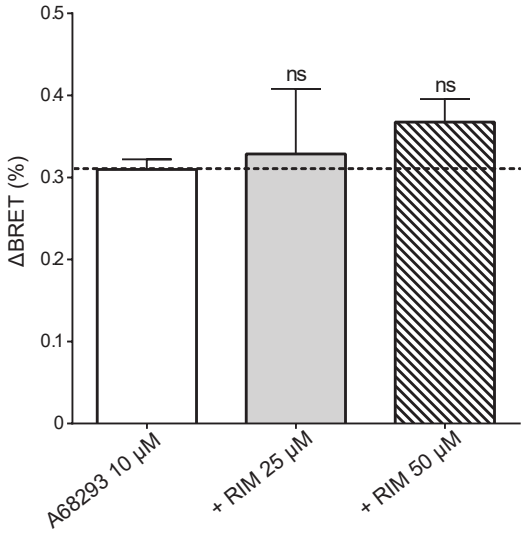
ΔBRET (%)
ns
ns
A68293 10 μM
+ RIM 25 μM
+ RIM 50 μM

Figure 6

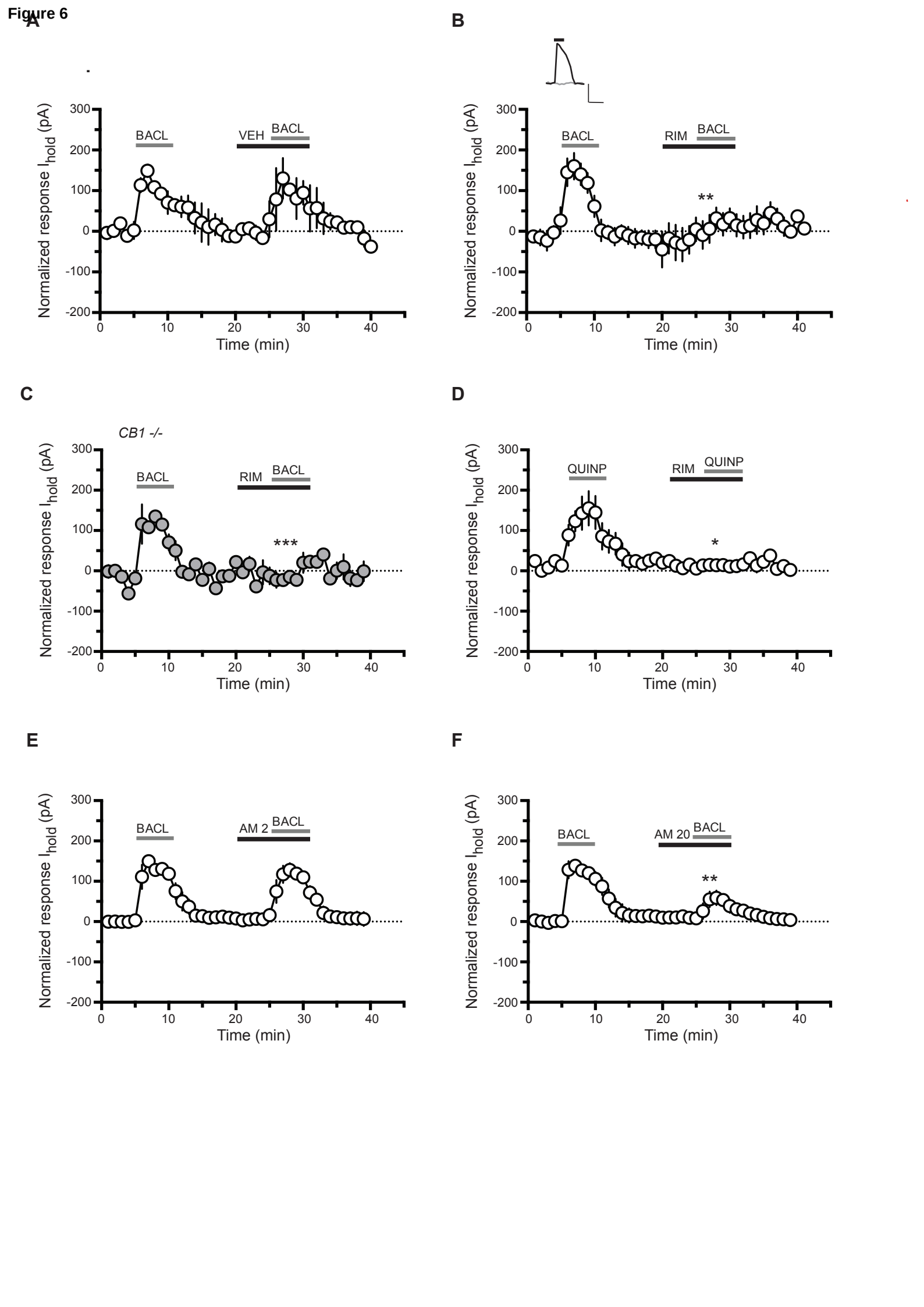
A
B
C
D
E
F
BACL
VEH
RIM
QUINP
AM 2
AM 20
CB1 -/-
Normalized response Ihold (pA)
Time (min)
**
***
*

Figure 7

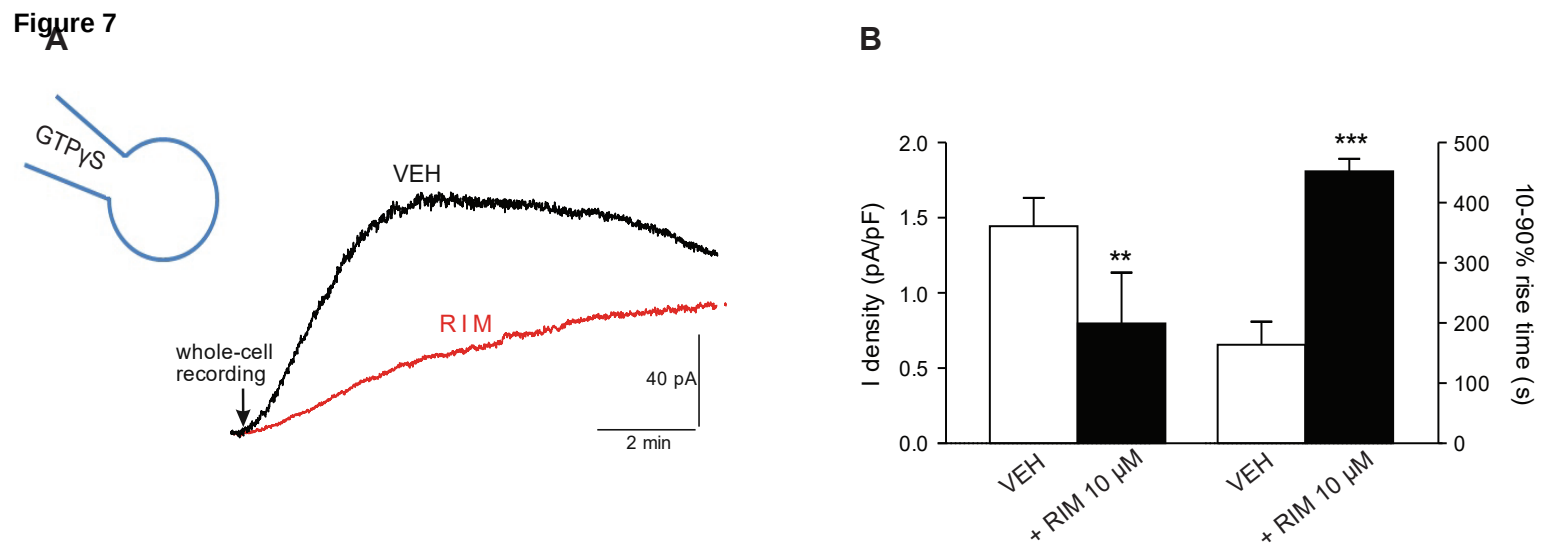
A
GTPγS
VEH
RIM
whole-cell
recording
40 pA
2 min
B
I density (pA/pF)
10-90% rise time (s)
2.0
1.5
1.0
0.5
0.0
500
400
300
200
100
0
**
***
VEH
+ RIM 10 μM
VEH
+ RIM 10 μM

Figure 8

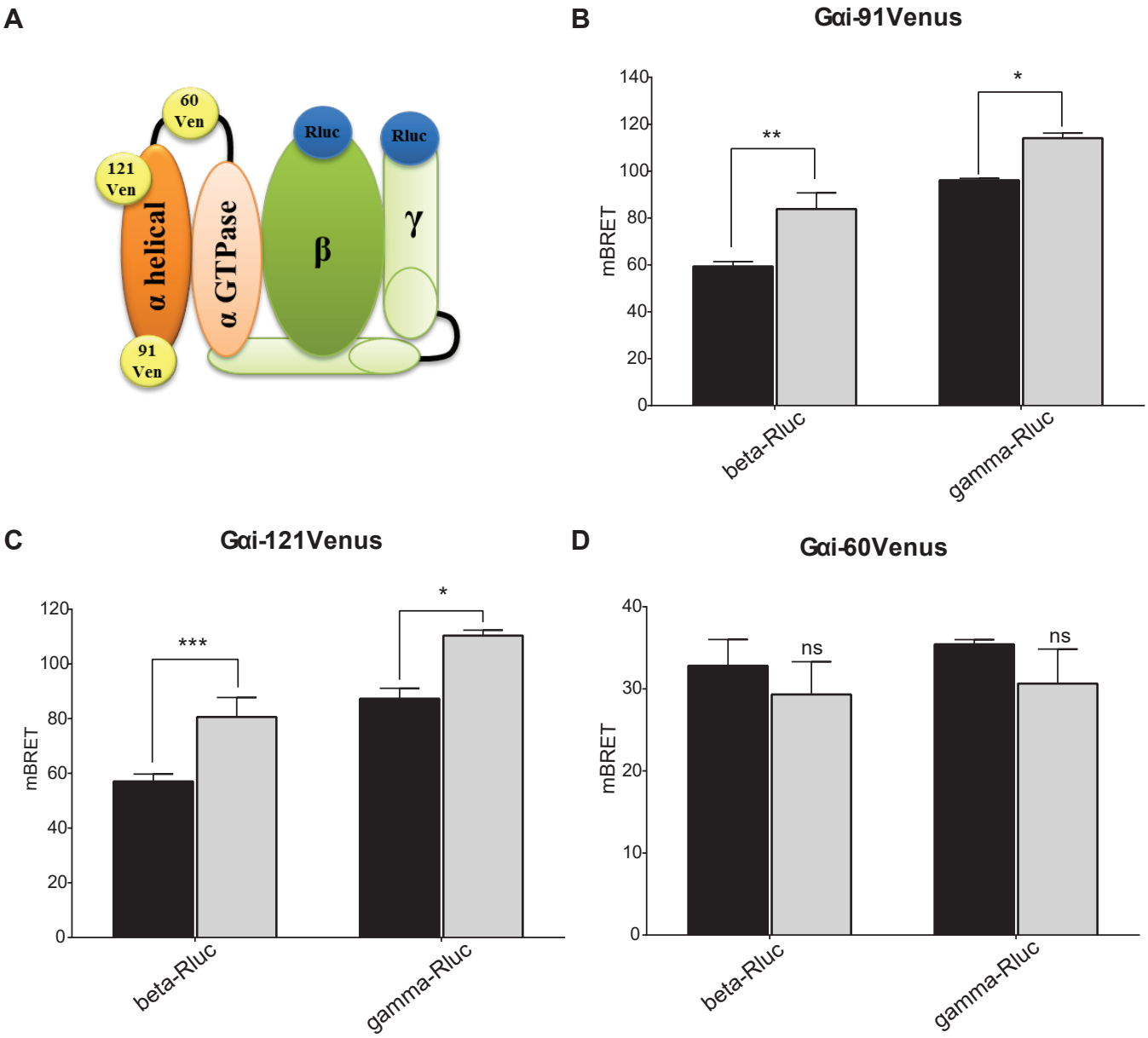
A
60 Ven
121 Ven
α helical
α GTPase
β
γ
Rluc
Rluc
91 Ven
B
Gαi-91Venus
mBRET
140
120
100
80
60
40
20
0
**
*
beta-Rluc
gamma-Rluc
C
Gαi-121Venus
mBRET
120
100
80
60
40
20
0
***
*
beta-Rluc
gamma-Rluc
D
Gαi-60Venus
mBRET
40
30
20
10
0
ns
ns
beta-Rluc
gamma-Rluc